

The threshold of semiconductor nanolasers

Marco Saldutti*, Yi Yu, and Jesper Mørk*

*DTU Electro, Technical University of Denmark, DK-2800 Kgs. Lyngby, Denmark and
NanoPhoton - Center for Nanophotonics, Technical University of Denmark, DK-2800 Kgs. Lyngby, Denmark*

(Dated: May 26, 2023)

Nanolasers based on emerging dielectric cavities with deep sub-wavelength confinement of light offer a large light-matter coupling rate and a near-unity spontaneous emission factor, β . These features call for reconsidering the standard approach to identifying the lasing threshold. Here, we suggest a new threshold definition, taking into account the recycling process of photons when β is large. This threshold with photon recycling reduces to the classical balance between gain and loss in the limit of macroscopic lasers, but qualitative as well as quantitative differences emerge as β approaches unity. We analyze the evolution of the photon statistics with increasing current by utilizing a standard Langevin approach and a more fundamental stochastic simulation scheme. We show that the threshold with photon recycling consistently marks the onset of the change in the second-order intensity correlation, $g^{(2)}(0)$, toward coherent laser light, irrespective of the laser size and down to the case of a single emitter. In contrast, other threshold definitions may well predict lasing in light-emitting diodes. These results address the fundamental question of the transition to lasing all the way from the macro- to the nanoscale and provide a unified overview of the long-lasting debate on the lasing threshold.

I. INTRODUCTION

Lasers exist in a myriad of forms and they are important for such a variety of scientific and technical applications that no list would barely do justice. Researchers are currently writing a new fascinating chapter in the exciting history [1] of laser development: nanolasers [2–5].

Nanolasers are compact and energy-efficient light sources that bring to the nanoscale the benefits and potentials of coherent light. Applications range from biochemical sensing [6] and quantum technologies [7, 8] to artificial intelligence and neuromorphic computing [9], to name a few. Nanolasers are also attractive for chip-scale optical communications [10, 11]. This new communication scheme, with information traveling through optical waveguides from chip to chip or even within a single chip, requires semiconductor light sources with ultra-small footprint, low noise and energy consumption of few femtojoules per bit or even less [12].

Emerging dielectric cavities comprising a bowtie geometry [13–18] confine light to an effective mode volume [19, 20] deep below the so-called diffraction limit [21–23] while keeping the quality factor (Q-factor) sufficiently high. As a result, these cavities with extreme dielectric confinement (EDC) can achieve strong light-matter interaction. In EDC cavities, the optical density of states is largely dominated by a single mode [18], thereby limiting the fraction of undesired spontaneous emission coupled into other modes. Therefore, EDC cavities are promising candidates as nanolasers with a near-unity

spontaneous emission factor (β -factor). EDC cavities may lead to nanolasers with ultra-low threshold current if nonradiative recombination is kept at bay [24] and good spatial and spectral overlap between the cavity field and the active material is ensured.

However, how to define the lasing threshold is far from obvious when the β -factor approaches unity [25]. In conventional macroscopic lasers, the transition from incoherent to coherent light is abrupt and occurs over a negligibly small current range. In this case, the onset of lasing and with it the threshold current, are defined unambiguously [26]. With increasing β -factor, however, the change in the light coherence is more and more gradual and neither the light-current characteristic nor the linewidth of the emission spectrum are sufficient indicators of lasing [27]. The variation of the intensity correlation with increasing current is presently recognized as essential to proving lasing [28–32], but this criterion is not free from pitfalls. When measuring the intensity correlation with a typical Hanbury–Brown–Twiss (HBT) setup [33], the intrinsic latency and jitter of the detection process, despite recent progress [34], may well limit the temporal resolution of the measurement to values larger than the laser coherence time, at least below and around the lasing threshold [30, 35]. These issues often make the identification of the lasing threshold in nanolasers ambiguous and prone to interpretation. Moreover, irrespective of the practical limitations of the measurement setup, truly coherent light, corresponding to a Poissonian photon number distribution, is only achieved at asymptotically large values of current, which precludes a unique definition of lasing threshold based on the intensity correlation. One may specify a threshold current high enough to reach a certain degree of coherence [36], but this stand, albeit pragmatic, does

* Correspondence email address: marsal@dtu.dk, jsm@dtu.dk

not elucidate the fundamental question of the transition to lasing. Such a question has recently received the attention of numerous publications [32, 37–41] and what emerges is a rather confusing picture.

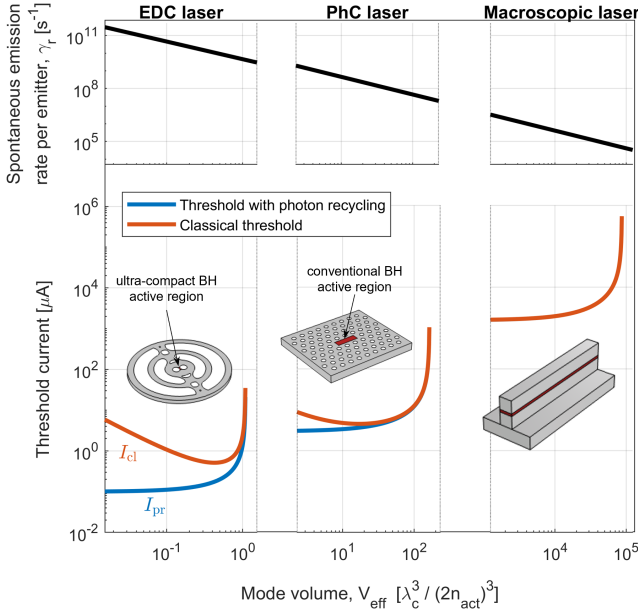


Figure 1. Spontaneous emission rate per emitter (top) and threshold current (bottom) versus mode volume for a nanolaser with extreme dielectric confinement (EDC laser, left), a photonic crystal laser (PhC laser, center) with a buried heterostructure (BH) active region and a conventional macroscopic laser (right). Both the threshold with photon recycling (blue) and the classical threshold (red) are shown. The number of emitters is fixed, while the mode volume varies with the optical confinement factor. Apart from the mode volume, the parameters are listed in Tab. I, with the EDC laser being EDC laser 1.

In this article, we propose a simple expression for the threshold current, valid all the way from the macro to the nanoscale. By incorporating the physics of photon recycling [42], this threshold extends to semiconductor nanolasers with a high β -factor, such as EDC lasers, the classical definition of balance between gain and loss [26, 43]. We name this generalized condition *threshold with photon recycling*. Importantly, the expression accounts for the finite number of electronic states available to the lasing process, which must be considered in the case of nanolasers.

As an example, Fig. 1 illustrates the spontaneous emission rate per emitter, γ_r (top), and the threshold current (bottom) versus mode volume for an EDC laser (left), a photonic crystal (PhC) laser (center) and a macroscopic laser (right). The carrier lifetime is $(\gamma_r + \gamma_{bg})^{-1}$, where γ_{bg} reflects nonradiative recombination and recombination into nonlasing modes. Importantly, γ_r is inversely proportional to the mode volume.

In macroscopic lasers, the threshold current with photon recycling, I_{pr} (blue), reduces to the classical definition of balance between gain and loss, I_{cl} (red). However, qualitative and quantitative differences between the two thresholds gradually emerge with decreasing mode volume. In EDC lasers, I_{cl} strongly increases when the mode volume becomes very small, due to the strong carrier lifetime reduction. Conversely, I_{pr} decreases and eventually saturates, due to an effective saturation of the carrier lifetime induced by photon recycling.

Importantly, the threshold with photon recycling consistently marks the onset of the transition toward coherent laser light. We demonstrate this property by studying the evolution of the photon statistics [25] with increasing current from below to above threshold. We consider both a conventional Langevin approach [26, 44] and a more fundamental stochastic simulation scheme [45, 46].

Besides the threshold with photon recycling, we scrutinize several other threshold definitions [32, 37, 39, 41, 47–49] and explicitly show that some of them are not reliable indicators of lasing. These definitions, such as the quantum threshold [47] and unlike the threshold with photon recycling, may well predict the possibility of lasing in structures that remain in the LED regime of thermal light at all pumping levels.

The article is organized as follows. In Sec. II, we review the physics of extreme dielectric confinement and clarify the mode volume definitions relevant to nanolasers. In Sec. III, we illustrate the laser model and discuss the two approaches utilized in this article to describe the quantum noise. In Sec. IV, we derive and analyze the threshold with photon recycling and thoroughly discuss the laser input-output characteristics, from the macro- to the nanoscale. We elucidate the role of the spontaneous emission factor, often misunderstood, in Sec. V and review other threshold definitions in Sec. VI. In Sec. VII, we focus on the photon probability distributions and another threshold definition [41] recently proposed. Finally, we summarize the discussion and draw the main conclusions in Sec. VIII. The appendices provide further details on the derivation of the spontaneous emission rate per emitter (Sec. IX) and the variance of the photon number from the Langevin approach (Sec. X).

II. EXTREME DIELECTRIC CONFINEMENT

Generally speaking, concentrating the light spatially and for a sufficiently long time is key to achieving strong light-matter interaction. The figures of merit reflecting the spatial and temporal confinement of light are the mode volume and the quality factor (Q-factor), respectively [50]. Plasmonics [51] may achieve deep

sub-wavelength optical confinement, but the absorption losses in metals severely limit the quality factor [52]. Photonic crystal (PhC) cavities [50, 53] can easily offer Q-factors of several thousands if not millions [54], but often have mode volumes exceeding $\lambda_c^3/(2n)^3$ by a factor of 2 or 3 [55], where $\lambda_c^3/(2n)^3$ sometimes is referred to as the diffraction-limited mode volume [21–23]. Here, λ_c is the vacuum wavelength and n is the material refractive index. Emerging cavities with extreme dielectric confinement (EDC) [13–18] promise the perfect blend of an ultra-small mode volume and a sufficiently high quality factor.

In particular, EDC cavities may achieve strong light-matter interaction without needing extremely high Q-factors. Without trading energy efficiency for speed, EDC cavities are excellent candidates for numerous applications where high energy efficiency and wide bandwidths are simultaneously desirable. These include few-photon nonlinearities [14] and quantum technologies [56, 57], photodetectors [58] and optical switches [59, 60], as well as nanoscale light-emitting diodes and nanolasers with squeezed intensity noise [61].

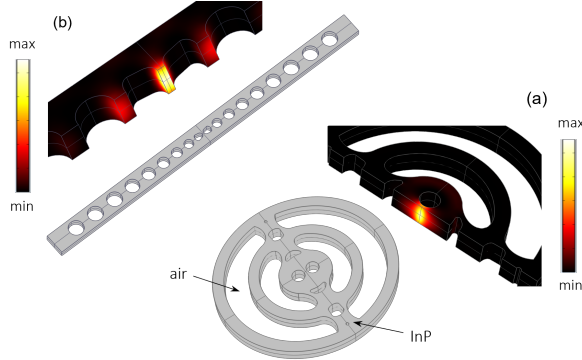


Figure 2. Optical cavities with extreme dielectric confinement (EDC) inspired by recently demonstrated designs [13–16, 18]. The color plots show the squared magnitude of the electric field, $|\mathbf{E}(\mathbf{r})|^2$, on a cross-section of the bowtie.

In EDC cavities, the spatial confinement of light is dictated by the boundary conditions of Maxwell's equations, requiring the normal component of the electric displacement field and the tangential component of the electric field to be continuous across a dielectric interface [62]. A bowtie geometry, as present in EDC cavities, properly leverages these two requirements, increasing the electric energy density around a given point. For example, Fig. 2 illustrates two EDC cavities inspired by recent designs [13–16, 18], with a bowtie located at the center. The rings (cf. Fig. 2a) or the holes (cf. Fig. 2b) surrounding the bowtie effectively act as a distributed Bragg grating, which suppresses the in-plane radiation loss and increases the Q-factor. The distance between

the holes forming the bowtie is of the order of a few nanometers [16, 18].

The relevant definition of mode volume depends on the specific type of light-matter interaction that is considered [53]. In lasers, stimulated and spontaneous emission scale with γ_r , the spontaneous emission rate per emitter. For lasers with discrete and identical two-level emitters, such as quantum dots with a dominant electronic transition and negligible inhomogeneous broadening, γ_r may be expressed as [44]

$$\gamma_r = \frac{2d^2}{\hbar\epsilon_0 n_{act}^2} \frac{\omega_c}{\gamma_2} \frac{1}{V_p} \quad (1)$$

In Sec. IX, we provide a detailed derivation of Eq. 1 on the basis of Fermi's golden rule. In Eq. 1, V_p is the mode volume and ω_c is the angular frequency of the lasing mode. The refractive index at the position of the emitters, n_{act} , and the emitter dipole moment, d , are taken to be the same for all the emitters. The dephasing rate, $\gamma_2 = 2/T_2$, reflects the emitter homogeneous broadening, with T_2 being the dephasing time. The emitters are assumed to be identical and in resonance with the lasing mode. Any detuning would limit γ_r , thereby effectively reducing the emitter dipole moment (for details, see Sec. IX).

To a first approximation, Eq. 1 is also valid for lasers with an extended active region. In this case, γ_2 may also reflect the inhomogeneous broadening of the gain material (for details, see Sec. IX). We note that Eq. 1 considers the so-called good-cavity limit [44], where the emitter broadening is larger than the cavity linewidth. This is the typical scenario of semiconductor lasers working at room temperature [63]. We also note that the light-matter coupling rate [46], g , is given by $\sqrt{\gamma_2 \gamma_r}/2$.

For nanolasers with a single emitter [46, 64], the mode volume appearing in Eq. 1 is expressed as [65]

$$\frac{1}{V_p} \rightarrow \frac{1}{V_{opt}} = \frac{\epsilon_0 n^2(\mathbf{r}_e) |\hat{\mathbf{d}}_e \cdot \mathbf{E}(\mathbf{r}_e)|^2}{\int_V \epsilon_0 n^2(\mathbf{r}) |\mathbf{E}(\mathbf{r})|^2 d^3 \mathbf{r}} \quad (2)$$

where \mathbf{r}_e is the position of the emitter, $\hat{\mathbf{d}}_e$ is the unit vector which represents the orientation of the emitter dipole and \mathbf{E} is the electric field of the lasing mode. We note that a rigorous definition should be based on the theory of quasi-normal modes [66, 67]. However, if the Q-factor is high enough, generalized definitions [19, 20] reduce to Eq. 2. The integration volume, V , should suitably enclose the physical volume of the cavity with a margin of a few wavelengths.

For nanolasers with an extended active region, the mode volume is expressed in a different manner. In this case, averaging over the active region (for details, see Sec. IX) leads to an *effective* mode volume

$$\frac{1}{V_p} \rightarrow \frac{1}{V_{eff}} = \frac{\Gamma}{V_{act}} \quad (3)$$

Here, V_{act} is the physical volume of the active region. The optical confinement factor, Γ , is the fraction of electric energy stored within the active region volume, that is

$$\Gamma = \frac{\int_{V_{act}} \epsilon_0 n_{act}^2 |\mathbf{E}(\mathbf{r}_e)|^2 d^3 \mathbf{r}_e}{\int_V \epsilon_0 n^2(\mathbf{r}) |\mathbf{E}(\mathbf{r})|^2 d^3 \mathbf{r}} \quad (4)$$

The active region refractive index, n_{act} , is assumed to be uniform throughout the active region. Eq. 3 is the usual definition of mode volume as encountered in the conventional theory of semiconductor lasers [26]. We note that Eq. 3 and Eq. 4 reduce to Eq. 2 if the active region volume is much smaller than the scale on which the electric field amplitude varies. Any non-perfect alignment between the electric field and the dipoles is considered by effectively reducing the emitter dipole moment in Eq. 1 (see Sec. IX).

Notably, a passive EDC cavity with a record mode volume, V_{opt} , around $0.08 \lambda_c^3 / (2n)^3$ has been demonstrated experimentally [16]. The cavity, designed by topology optimization [15, 68], is similar to that in Fig. 2a. The mode volume is evaluated at the center of the cavity by assuming perfect alignment between the emitter dipole and the cavity field.

Future designs may specifically target nanolaser applications. In particular, designs optimizing the optical confinement factor in a small active region, as enabled by the buried heterostructure technology [69, 70], may lead to EDC lasers with an ultra-low threshold current.

III. LASER MODEL

We model the laser by rate equations for the average number of excited emitters (carriers), n_e , and the average number of photons in the lasing mode, n_p [44]:

$$\frac{dn_e}{dt} = \frac{I}{q} \left(1 - \frac{n_e}{n_0}\right) - \gamma_r(2n_e - n_0)n_p - (\gamma_r + \gamma_{bg})n_e \quad (5)$$

$$\frac{dn_p}{dt} = \gamma_r(2n_e - n_0)n_p + \gamma_r n_e - \gamma_c n_p \quad (6)$$

Here, I is the injection current, n_0 is the total number of emitters and q is the electron charge. The net stimulated emission rate, $\gamma_r(2n_e - n_0)n_p$, is the difference between the stimulated emission rate, $\gamma_r n_e n_p$, and the stimulated absorption rate, $\gamma_r(n_0 - n_e)n_p$. The spontaneous emission rate into the lasing mode, $\gamma_r n_e$, coincides with the stimulated emission rate with one photon in the mode, as following from Einstein's relation [43, 63, 71, 72]. Nonradiative recombination and radiative recombination into non-lasing modes are embedded into the background recombination rate, γ_{bg} . The photon decay rate, accounting for intrinsic and

mirror losses, is denoted by γ_c and determines the Q-factor, $Q_c = \omega_c / \gamma_c$. The total decay rate per emitter is $\gamma_t = \gamma_r + \gamma_{bg}$, whereas the pump rate per emitter is $\gamma_p = I / (qn_0)$.

We define the spontaneous emission factor (β -factor) as the ratio between the spontaneous emission rate into the lasing mode and the total carrier recombination rate [25, 35, 44]:

$$\beta = \frac{\gamma_r n_e}{\gamma_r n_e + \gamma_{bg} n_e} = \frac{\gamma_r}{\gamma_r + \gamma_{bg}} \quad (7)$$

Therefore, the β -factor herein defined also reflects the impact of nonradiative recombination and quantifies the overall efficiency of carrier recombination into the lasing mode.

Eq. 5 and Eq. 6 are derived from cavity quantum electrodynamics models of discrete, two-level emitters [73–75] by adiabatic elimination of the medium polarization and by neglecting correlations between emitters. Therefore, as for conventional [26] rate equations, coherent effects such as Rabi oscillations [46, 76] and superradiance [77] are not included. However, as opposed to conventional rate equations, we include the pump blocking term, $(1 - n_e / n_0)$, which represents Pauli-blocking and reflects the finite number of emitters [44].

To a first approximation, the equations also apply to semiconductor lasers with extended active media, such as layers of quantum wells [35, 70, 78] or quantum dots [79, 80]. In this case, the inhomogeneous broadening of the electronic transitions, as described by the electronic density of states [26], generally makes the stimulated and spontaneous emission rates nonlinear functions of the number of carriers. Therefore, more accurate modeling requires purely numerical approaches [35, 63, 81]. However, if the injection level is not much higher than the transparency condition, the spontaneous and stimulated emission rates are approximately linear in the number of carriers, as entailed by Eq. 5 and Eq. 6 and often assumed in the literature [43, 70, 78, 79]. In the case of extended active media, the pump blocking term effectively reflects the saturation [81] with increasing current of the number of electron-hole pairs interacting with the cavity field. These electronic states are located in a bandwidth typically determined by the homogeneous broadening and centered around the cavity mode frequency [82] (cf. Eq. 32 and Eq. 35 in Sec. IX). In the absence of other modes, the number of electronic states which may contribute to lasing is bound to saturate as the quasi-Fermi levels of electrons and holes move past the cavity mode transition. We note that the single mode approximation is particularly appropriate in EDC cavities [18].

The rate equations govern the average number of photons and carriers, but the intrinsic quantum noise induces fluctuations around these averages. As a result, laser light possesses characteristic statistical properties,

depending on the pumping level. In the following, we briefly illustrate two techniques to model the quantum noise: the Langevin approach [26] and a recently developed stochastic approach [45].

By following the Langevin approach, we add Langevin noise forces to Eq. 5 and Eq. 6 and carry out a small-signal analysis. Hence, we compute the fluctuation in the photon number and the corresponding power spectral density [26]. By integrating the spectral density over all frequencies, we calculate the variance of the photon number, $\langle \Delta n_p^2 \rangle$. The expression of this variance depends on the small-signal coefficients of the rate equations and the correlation strengths of the Langevin noise forces, as well as the pumping level (for details, see Sec. X). From the variance, we readily obtain the relative intensity noise, RIN, the Fano factor [25], F_F , and the second-order intensity correlation, $g^{(2)}(0)$ [33]:

$$\text{RIN} = \frac{\langle \Delta n_p^2 \rangle}{\langle n_p \rangle^2}, \quad F_F = \frac{\langle \Delta n_p^2 \rangle}{\langle n_p \rangle}, \quad g^{(2)}(0) = \frac{\langle n_p(n_p - 1) \rangle}{\langle n_p \rangle^2} \quad (8)$$

The average of the photon number, $\langle n_p \rangle$, is calculated analytically from the carrier and photon rate equations. Since the variance may be expressed as $\langle \Delta n_p^2 \rangle = \langle n_p^2 \rangle - \langle n_p \rangle^2$, one finds $g^{(2)}(0) = 1 + \text{RIN} - 1/\langle n_p \rangle$. It should be stressed that here we focus on the statistical properties of the intracavity photon number. The output optical power is affected by an additional noise contribution, the partition noise [26] at the laser output. As a result, the variance of the photon number and the variance of the output power generally differ [26, 46, 61, 83].

The Langevin approach is the standard technique to model the quantum noise. However, describing the quantum noise with Langevin noise sources is questionable in the case of very few emitters [46, 84]. Indeed, by definition, the small-signal analysis assumes the quantum fluctuations to be a small perturbation of the state of the laser. In nanolasers, variations on the order of a single photon or a single emitter excitation may constitute a non-negligible perturbation, due to the small number of photons and carriers. Hence, a small-signal analysis is not guaranteed to properly describe the noise properties.

Instead of modeling the *collective* effect of the photon and carrier fluctuations with Langevin noise forces, the stochastic approach more fundamentally describes the laser dynamics as a stochastic Markov process in the space of the photon and carrier numbers [45]. More specifically, the Langevin approach describes the number of photons and carriers as *continuous* time variables. On the contrary, the stochastic approach reflects the shot noise affecting photons and carriers by considering the latter as *discrete* stochastic time variables. The shot noise originates from the finite values of the electronic charge and the photon energy, imposing a granularity on the electron current and the optical power. The

rates of the various events involving emitters and photons (stimulated emission, spontaneous emission, etc.) are regarded as probabilities per unit of time that a given event would occur, based on the current number of particles. How long it takes for the next event to occur and which event it occurs is determined via a Monte Carlo simulation framework, the so-called Gillespie's first reaction method [85]. The number of photons and carriers is resolved versus time with a nonuniform time step. Compared to similar stochastic approaches with fixed time increment [44, 61, 86], Gillespie's first reaction method is numerically exact, in the sense that it does not require any convergence study on the width of the time step [45]. The average photon number and the photon variance are obtained from the time-resolved number of photons. Subsequently, one finds the relative intensity noise, the Fano factor and the intensity correlation.

In general, good agreement is found between the Langevin approach and the stochastic approach when considering the average photon number and the relative intensity noise, even in the presence of very few emitters [44, 45] and down to the case of a single emitter [46]. Qualitative discrepancies, though, may emerge in the intensity correlation [46] and the Fano factor, as illustrated later on in Sec. VII. For a single emitter, for instance, the stochastic approach, contrary to the Langevin approach, well reproduces the change in the intensity correlation with increasing current as obtained from full quantum simulations [46].

Finally, a comment is due on the impact of pump broadening. The incoherent pumping leads to pump-induced dephasing, effectively increasing the emitter dephasing rate [75, 87]. As a result, the spontaneous emission rate per emitter may be quenched at high current values. However, the effect is negligible if the pumping rate per emitter, γ_p , is much smaller than the nominal value of γ_2 . Therefore, one can safely ignore pump broadening if considerations are limited to values of current much smaller than $I_{pb} = qn_0\gamma_2$.

Throughout this article, we assume $d = 10^{-28}$ Cm [44, 88], $n_{act} = 3.3$, $\lambda_c = 1.55\ \mu\text{m}$ and $T_2 = 50\ \text{fs}$. The value of the dephasing time, in the range of a few tens of femtoseconds, reflects operation at room temperature [89]. Unless explicitly noted, pump broadening would not affect the results herein discussed and is therefore neglected.

IV. THRESHOLD WITH PHOTON RECYCLING

Despite decades of research, the concept of lasing threshold in semiconductor micro- and nanolasers is still the center of a vivid debate [25, 27, 32, 36–41, 43, 47–49, 72]. As we shall see, the large spontaneous emis-

sion rate per emitter achievable in EDC lasers questions the standard approach [26] for calculating the threshold current. In the following, we generalize the classical definition of balance between gain and loss by building on the concept of photon recycling [42].

Classically, the lasing threshold is reached when the *net* stimulated emission, $\gamma_r(2n_e - n_0)n_p$, balances the optical loss, $\gamma_c n_p$. This balance requires the number of carriers to be

$$n_{e_{th}} = \frac{n_0}{2} + \frac{\gamma_c}{2\gamma_r} \quad (9)$$

Here, the first term is the number of carriers at transparency and the second is the additional fraction one needs to excite to compensate for the cavity loss. In the presence of lasing, the number of carriers is clamped at $n_{e_{th}}$.

The transparency current is defined unambiguously. By substituting the number of carriers at transparency into the rate equations, one finds the number of photons at transparency

$$\xi = \frac{n_0 \gamma_r}{2 \gamma_c} = N_{tr} \Gamma \frac{2d^2}{\hbar \epsilon_0 n_{act}^2} \frac{Q_c}{\gamma_r} \quad (10)$$

and the transparency current

$$I_{tr} = q \frac{2\xi \gamma_c}{\beta} \quad (\text{transparency}) \quad (11)$$

In Eq. 11, the factor of 2 is absent if pump blocking is neglected. In the last step of Eq. 10, we have assumed an extended active region and expressed the total number of emitters as $n_0 = 2N_{tr}V_{act}$, with N_{tr} being the transparency carrier density.

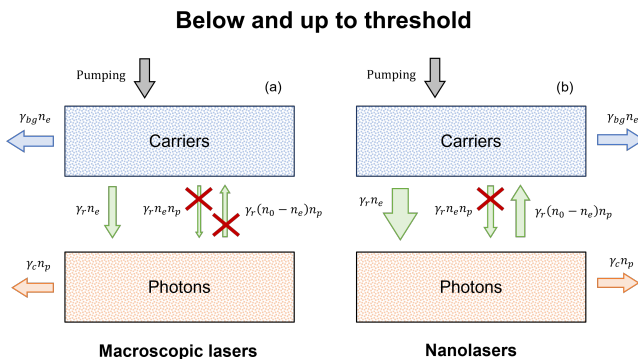


Figure 3. Major contributions to the carrier and photon dynamics below and up to threshold in (a) macroscopic lasers and (b) nanolasers. The processes marked with a cross have a minor impact. In nanolasers, for β approaching one and ξ sufficiently larger than one-half, a large fraction of the photons funneled into the lasing mode are re-absorbed before decaying, leading to photon recycling.

As opposed to the transparency current, the threshold current is not necessarily a well-defined quantity. Indeed, a quick inspection of the photon rate equation shows that the balance between gain and loss is only achieved, strictly speaking, in the limit of an infinite number of photons, due to spontaneous emission into the lasing mode. The standard approach [26] is to estimate the number of carriers below threshold by wholly neglecting the net stimulated emission term in the carrier rate equation, as illustrated by Fig. 3a. Thus, by requiring the number of carriers to fulfill Eq. 9, one finds the classical threshold current, $I_{cl} = q(1 - n_{e_{th}}/n_0)\gamma_t n_{e_{th}}$, with $\gamma_t = \gamma_r + \gamma_{bg}$. The term in brackets is due to pump blocking, often neglected [26, 43], and $\gamma_t n_{e_{th}}$ is the total loss rate of carriers at threshold.

By introducing the number of photons at transparency, one finds

$$I_{cl} = \frac{q}{\eta} \frac{\gamma_c}{2\beta} (2\xi + 1) \quad (\text{classical threshold}) \quad (12)$$

where the pump injection efficiency, η , is

$$\eta = \frac{1 - 1/(2\xi)}{2} \quad (13)$$

We emphasize that η reflects the leakage due to pump blocking. If pump blocking is neglected, then $\eta = 1$. Any additional leakage would further degrade the injection efficiency by a factor η_i [26], amounting to quantitative, but not qualitative changes. For simplicity, we assume $\eta_i = 1$ throughout this article.

Importantly, in the presence of pump blocking, the maximum available gain is finite ($n_0 \gamma_r$). Therefore, according to the classical definition, lasing is unattainable if $n_0 \gamma_r \leq \gamma_c$, namely

$$\xi \leq \frac{1}{2} \quad (\text{LED regime}) \quad (14)$$

In this case, the laser operates as a light-emitting diode (LED) and the photon number saturates at sufficiently high currents. This saturation is a characteristic feature of LEDs, though in practice other detrimental effects herein neglected, such as the temperature increase, may cause a similar saturation even in lasers.

The standard approach to estimate the number of carriers below threshold is invalid if the β -factor is close to one. In this case, due to the large spontaneous emission into the lasing mode, the number of photons below transparency may be non-negligible. Furthermore, if ξ is sufficiently larger than one-half, a generated photon has a higher chance of being re-absorbed than decaying. Indeed, ξ is one-half of the ratio between the stimulated absorption rate well-below inversion, $\gamma_r n_0 n_p$, and the photon decay rate, $\gamma_c n_p$. This process of large spontaneous emission into the lasing mode and significant

stimulated re-absorption recycles the generated photons without major energy loss and effectively increases the carrier lifetime [42].

We have found that a better estimate of the number of carriers below threshold in the presence of photon recycling is obtained by neglecting the stimulated emission, but retaining the stimulated absorption, as illustrated by Fig. 3b. In other terms, we assume $\gamma_r(2n_e - n_0)n_p \approx -\gamma_r n_0 n_p$ in both the carrier and photon rate equations, leading to

$$n_e \approx \frac{(I/q)(2\xi + 1)}{\gamma_r/\beta_{\text{eff}} + (2\xi + 1)\gamma_p} \quad (\text{below threshold}) \quad (15)$$

Here, we define an effective β -factor

$$\beta_{\text{eff}} = \frac{\beta}{1 + 2\xi(1 - \beta)} \quad (16)$$

Then, we require the approximate number of carriers from Eq. 15 to reach the level set by the gain-loss balance condition, $n_{e_{th}}$. This requirement leads to an expression for the threshold current including the effect of photon recycling, namely

$$I_{pr} = \frac{q}{\eta} \frac{\gamma_c}{2\beta_{\text{eff}}} \quad (\text{threshold with photon recycling}) \quad (17)$$

As illustrated by Fig. 1, our new expression, Eq. 17, and the classical expression, Eq. 12, coincide for $\beta \ll 1$ (macroscopic lasers), but differ qualitatively for β approaching 1 (EDC lasers). At the end of this section, we will return to this point in more detail.

Device	n_0	$V_p [\lambda_c^3/(2n_{act})^3]$	$Q_c [2.43 \times 10^3]$	$\gamma_{bg} [10^9 \text{ s}^{-1}]$
EDC laser 1	120	0.154	1	1
PhC laser	1.8×10^4	23.16	1	1
macroscopic laser	9.6×10^6	1.23×10^4	1	1
EDC laser 2	120	0.154	10	1
EDC laser 3	120	0.154	10	100
EDC laser 4	120	0.154	1	100
EDC laser 5	120	1	1	1
EDC laser 6	1	0.01	10	1
nanoLED A	120	1.54	1	1

Table I. Parameters of the main devices considered in this article: total number of emitters (n_0), mode volume (V_p), quality factor (Q_c) and background recombination rate (γ_{bg}).

To illustrate the role of photon recycling, we consider an EDC laser, namely EDC laser 1 in Tab. I. The number of emitters, n_0 , reflects a BH active region having a typical transparency carrier density of 10^{18} cm^{-3} , an area of $50 \times 50 \text{ nm}^2$ and 3 active layers, each being 8 nm thick. The mode volume follows from the active region volume and a total optical confinement factor equal to 3%, according to Eq. 3. These parameters lead to $\beta \approx 0.97$ and $\xi \approx 3.54$. Fig. 4 shows the number of carriers (solid) versus current, as well as the estimates with

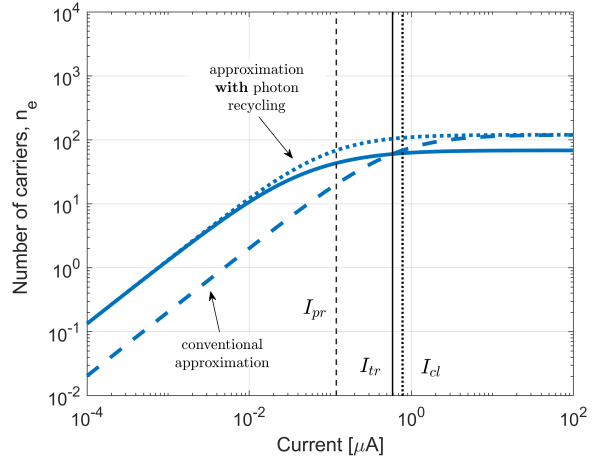


Figure 4. Number of excited carriers of EDC laser 1 in Tab. I versus current (solid). The conventional approximation used for calculating the threshold current (dashed) and our approximation with the inclusion of photon recycling (dotted, cf. Eq. 15) are also shown. The carriers start clamping at the threshold current with photon recycling, I_{pr} , even before reaching the transparency current, I_{tr} . The classical threshold current, I_{cl} , is slightly larger than I_{tr} .

(dotted) and without (dashed) photon recycling. The vertical lines pinpoint the threshold current with photon recycling (dashed), the transparency current (solid) and the classical threshold current (dotted).

Eq. 15 well describes the number of carriers below the threshold with photon recycling. Importantly, it is seen that the number of carriers at a given current below transparency is higher than expected from the conventional approximation. This discrepancy is due to photon recycling, which effectively increases the carrier lifetime. As a result, a lower current suffices to reach the number of carriers required by the gain-loss balance condition. We emphasize that the large fraction of spontaneous emission into the lasing mode plays a key role, unlike the usual regime encountered in macroscopic lasers. As further discussed in Sec. V and shown in Fig. 4, the threshold with photon recycling may well be attained below transparency. In such a case, the net stimulated emission term is negative. Therefore, the growth of the photon number is largely sustained by the spontaneous emission into the lasing mode.

We shall now examine the variation with current of the average photon number, the laser linewidth and the photon statistics, including key figures of merit such as the relative intensity noise (RIN), the Fano factor and the intensity correlation, introduced in Sec. III. Besides EDC laser 1, we consider a PhC laser and a macroscopic laser, with parameters summarized in Tab. I. The number of emitters reflects an active region with a typical transparency carrier density of 10^{18} cm^{-3} and consisting of 3 active layers, each being 8 nm thick and

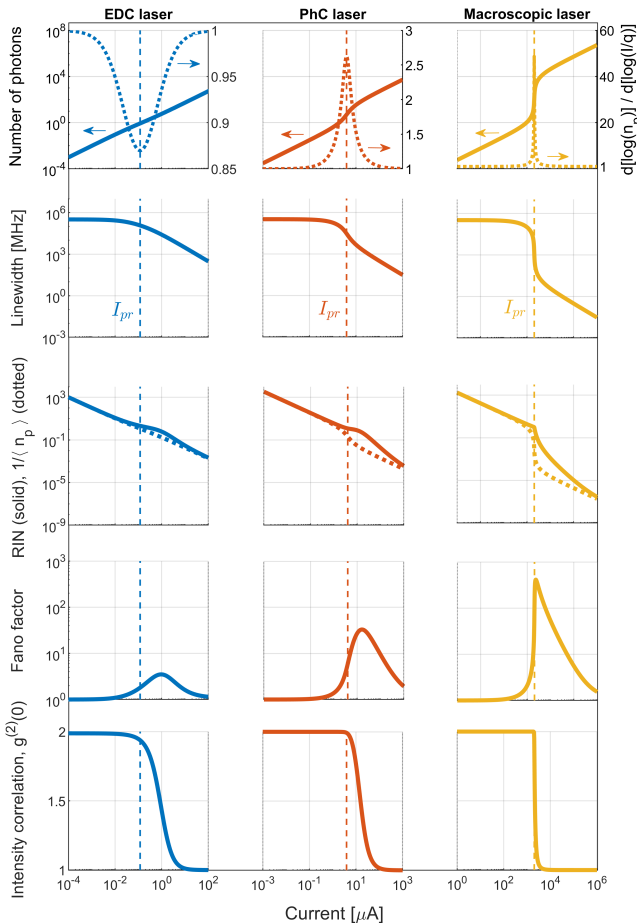


Figure 5. Input-output characteristics of a nanolaser with extreme dielectric confinement (EDC laser, left), a photonic crystal laser (PhC laser, center) and a conventional macroscopic laser (right). The parameters for the EDC laser (EDC laser 1) as well as the PhC and macroscopic laser are given in Tab. I. The vertical, dashed lines indicate the threshold with photon recycling.

having an area of $0.3 \times 1.25 \mu\text{m}^2$ [32] (PhC laser) and $2 \times 100 \mu\text{m}^2$ [26] (macroscopic laser). The mode volume corresponds to a total optical confinement factor equal to 3%, leading, in all cases, to the same value of ξ (cf. Eq. 10). Fig. 5 illustrates the input-output characteristics of the EDC laser (left), the PhC laser (center) and the macroscopic laser (right). The vertical, dashed lines indicate the threshold with photon recycling. The quantum noise (see Sec. III) is modeled by the Langevin approach, but we note that the stochastic approach would provide similar results. Deviations emerge when further scaling down the number of emitters, as illustrated explicitly in Sec. VII.

In the first row of Fig. 5, the light-current (LI) characteristic is displayed (left axis). The macroscopic laser features a marked intensity jump, with a typical S-shape

and a steep increase in the photon number at the threshold with photon recycling. The intensity jump reduces significantly for the PhC laser, whereas the EDC laser features an almost linear characteristic. As thoroughly discussed in Sec. V, the intensity jump scales with the inverse of the effective β -factor. Here, we point out that the threshold with photon recycling marks the inflection point of the LI characteristic on a double logarithmic scale. In other terms, it can be shown

$$\frac{d^2[\log(n_p)]}{d[\log(I/q)]^2} \Big|_{I_{pr}} = 0 \quad (18)$$

This key property makes the threshold with photon recycling a useful operational definition rather than a mere theoretical construction. We emphasize, though, that the threshold with photon recycling remains well defined (cf. Eq. 17) even in the case of a perfectly linear LI characteristic. In the first row of Fig. 5, the first derivative, $d[\log(n_p)]/d[\log(I/q)]$, is also shown (right axis). Consistently with Eq. 18, the threshold with photon recycling coincides with the maximum or the minimum of the first derivative, depending on whether the LI characteristic features a typical or an inverse [35] S-shape, respectively. The shape of the LI characteristic is further discussed in Sec. V.

The second row of Fig. 5 shows the laser linewidth, which we calculate by the modified Schawlow–Townes formula [26, 90]

$$\Delta\nu = \frac{\gamma_r n_e}{4\pi n_p} = \frac{\gamma_c}{4\pi} \frac{\xi + \frac{1}{2}}{n_p + \frac{1}{2}} \quad (19)$$

The Schawlow–Townes linewidth determines the intrinsic coherence time of the laser light, limited by fluctuations induced by spontaneous emission on the phase of the electric field. The original formula derived by Schawlow and Townes [91] applies well below threshold and it is a factor of two larger than Eq. 19. Well above threshold, instead, the intensity fluctuations are quenched and only phase fluctuations are important [90], leading to Eq. 19. We note that in the presence of gain-induced refractive index modulation, herein neglected, the Schawlow–Townes linewidth should be multiplied by an additional factor of $1+\alpha^2$, with α being the linewidth enhancement factor [26, 92]. Furthermore, the linewidth may generally reflect additional effects, such as non-orthogonality of modes and bad-cavity effects [93, 94]. Nonetheless, Eq. 19 retains the fundamental dependence on the number of photons. Well below threshold, where the photon number is negligible, the linewidth is the same irrespective of the laser size, since all lasers in Fig. 5 feature the same value of ξ . Above threshold, instead, significant differences are found. In the macroscopic laser, the linewidth abruptly decreases at threshold, reflecting the marked intensity

jump. On the contrary, a gradual linewidth reduction is observed for the EDC and the PhC lasers. In this case, the narrowing sets in around the threshold with photon recycling, as also found by quantum simulations of single-emitter nanolasers [46].

The third row of Fig. 5 displays the relative intensity noise (solid) and the inverse of the average photon number (dotted). Well below threshold, the lasers operate as LEDs, hence generating thermal light. The variance is $\langle \Delta n_p^2 \rangle = \langle n_p \rangle^2 + \langle n_p \rangle$ [33] and the relative intensity noise reduces to $\text{RIN} = 1 + 1/\langle n_p \rangle \approx 1/\langle n_p \rangle$. The approximation holds due to the very small average photon number. Well above threshold, the photon statistics asymptotically approaches a Poisson process, corresponding to coherent laser light. For a Poisson process, the variance equals the average [33], $\langle \Delta n_p^2 \rangle = \langle n_p \rangle$, leading to $\text{RIN} = 1/\langle n_p \rangle$. At intermediate pumping levels, the photon statistics is more blurred and the RIN is enhanced above the level of $1/\langle n_p \rangle$. Interestingly, a weaker enhancement is observed in the EDC laser.

In the fourth row of Fig. 5, the Fano factor is shown. Irrespective of the laser size, the Fano factor increases around threshold and decreases at larger current values. For the macroscopic laser, the maximum of the Fano factor coincides with the lasing threshold [25]. This motivates an alternative definition of threshold current, corresponding to the maximum of the Fano factor [48] (see Sec. VI). For the EDC laser and the PhC laser, instead, a much smoother increase is observed and the Fano factor peaks at a pumping level above the threshold with photon recycling. In addition, the maximum value of the Fano factor is seen to scale with the laser size. The EDC laser features the Fano factor with the lowest peak, signifying fluctuations in the photon number, at this current value, with the smallest amplitude relative to the average. This is ultimately due to the larger damping rate of EDC lasers (not shown in the figure). The damping rate determines the lifetime of a given noise fluctuation and, consequently, the level of noise accumulation. Therefore, in spite of the larger relative intensity noise above threshold, EDC lasers are expected to be more dynamically stable, as generally argued for nanolasers with a high β -factor [39, 95].

Finally, we consider the second-order intensity correlation, in the last row of Fig. 5. As the current grows from below to above threshold, the intensity correlation changes from $g^{(2)}(0) \approx 2$, well below threshold, to $g^{(2)}(0) \approx 1$, well above threshold, reflecting the change from thermal to Poissonian statistics. For the macroscopic laser, the change in the intensity correlation is very steep and sharply localized at threshold. For the EDC laser and the PhC laser, instead, a much more gradual variation is observed. In this case, the threshold with photon recycling marks the onset of the change in the intensity correlation.

To further characterize the significance of the thresh-

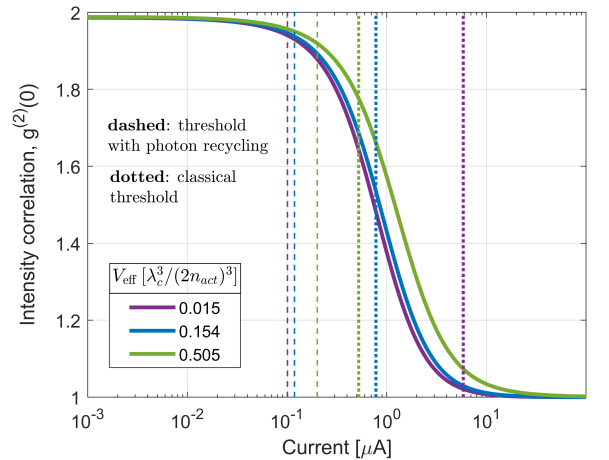


Figure 6. Intensity correlation versus current of EDC laser 1 in Tab. I (blue) and two other EDC lasers, with a smaller (purple) and a larger (green) mode volume, as indicated in the legend. The other parameters are the same as EDC laser 1. The vertical lines indicate the threshold current with photon recycling (dashed) and the classical threshold current (dotted).

old with photon recycling, in Fig. 6 we show the intensity correlation of two other EDC lasers, with a smaller (purple) and a larger (green) mode volume compared to EDC laser 1 (blue). The other parameters are unchanged. Irrespective of the mode volume, the threshold with photon recycling (dashed) consistently marks the onset of the transition toward coherent laser light. A smaller mode volume translates into better coherence at a given value of current and therefore into a lower threshold current with photon recycling. On the contrary, the classical threshold current (dotted) features the opposite trend.

We shall now reconsider Fig. 1, illustrating (bottom row) the threshold current versus mode volume. In each case (EDC, PhC and macroscopic laser), the mode volume reflects a total optical confinement factor ranging from 0.3% to 30%. In macroscopic lasers, one finds $\gamma_r \ll \gamma_{bg}$, leading to $\beta \ll 1$. As a result, the effective β -factor in Eq. 16 reduces to $\beta/(2\xi + 1)$ and the threshold with photon recycling approaches the classical threshold. At sufficiently small mode volumes, corresponding to $\xi \gg 1/2$ and $\beta_{\text{eff}} \approx \beta/(2\xi)$, the threshold current ultimately approaches the transparency current, Eq. 11. Since the carrier lifetime, $(\gamma_r + \gamma_{bg})^{-1}$, is dominated by the background recombination, the transparency current is independent of the mode volume and the threshold current saturates.

Conversely, the two thresholds differ qualitatively as the β -factor approaches 1, as is the case for EDC lasers. In this case, one finds $\gamma_r \gg \gamma_{bg}$, implying that γ_r determines the carrier lifetime. As a result, at suffi-

ciently small mode volumes, the classical threshold current strongly increases with decreasing mode volume, reflecting the growth of the transparency current. We note that the transparency current is the lower bound to the classical threshold current, consistently with the commonly accepted requirement [26] of inverting the active medium before achieving lasing. On the other hand, the effective β -factor reduces to $\beta \approx 1$ for β approaching 1. Correspondingly, one finds $\eta \approx 1/2$ if ξ is sufficiently larger than one-half. Ultimately, the threshold current with photon recycling tends to $I_{pr} \approx q\gamma_c$, thus being only limited by the cavity decay rate. Therefore, I_{pr} saturates in EDC lasers at sufficiently small mode volumes. As already mentioned in Sec. I, this behavior is interpreted as an effective saturation of the carrier lifetime induced by photon recycling.

We note that, irrespective of the β -factor and similarly to the classical threshold current, I_{pr} diverges if ξ tends to one-half, signifying the transition toward the LED operation regime. This is due to the inability of the given number of emitters and spontaneous emission rate per emitter, γ_r , to overcome the cavity loss. Therefore, the optimum mode volume minimizing the classical threshold current in EDC lasers is a trade-off between the larger transparency current and the higher pump injection efficiency with decreasing mode volume.

It should be mentioned that expressions similar to I_{pr} have been reported in previous works [32, 49, 72], but solely based on the empirical consideration of the second-order derivative of the average photon number [32] (cf. Eq. 18) or as ad-hoc definitions [49, 72]. Here, instead, we have elucidated the physical origin of this threshold definition. Moreover, we emphasize that pump blocking, neglected in those works, is essential to include to capture phenomena such as the appearance of an inverse S-shape in the LI characteristic (see Sec. V) or the transition with decreasing ξ from the laser regime to the LED regime, where no threshold exists.

V. ROLE OF THE SPONTANEOUS EMISSION FACTOR

The spontaneous emission factor or β -factor (cf. Eq. 7) quantifies the fraction of spontaneous emission funneled into the lasing mode. Generally speaking, a higher β -factor translates, below threshold, into a larger number of photons at a given current, thereby improving the energy efficiency [96]. In this section, we take a closer look at the impact of the β -factor on the LI characteristic and the threshold with photon recycling and clarify some common misconceptions.

As long as the cavity is much larger than the wavelength, the β -factor is mainly determined by the number of longitudinal modes in the spontaneous emission bandwidth [26, 72]. In this case, the β -factor is

smaller than one [26] and increases with decreasing cavity length due to the larger free spectral range. However, as the dimensions of the cavity become comparable to the wavelength, the density of optical modes per unit frequency and unit volume departs [97–100] from its simple bulk form [26], just as for the electronic density of states in the case of quantum wells and quantum dots. This leads to a nontrivial dependence of the spontaneous and background recombination rates on the cavity geometry. If properly engineered, nanolasers may have a near-unity [35, 79] β -factor, unlike the case of conventional macroscopic lasers.

It should be mentioned, though, that the spontaneous and background recombination in the case of inhomogeneously broadened active media also depend on the electronic density of states and, nonlinearly, on the pumping level, as detailed in Sec. IX. As a result, the β -factor in lasers with extended active media is also a function of the number of carriers [63, 81]. In general, it should be stressed that the β -factor may be either suppressed or enhanced, depending on the optical density of states, the electronic density of states and their frequency overlap [101–103], as well as on the pumping level.

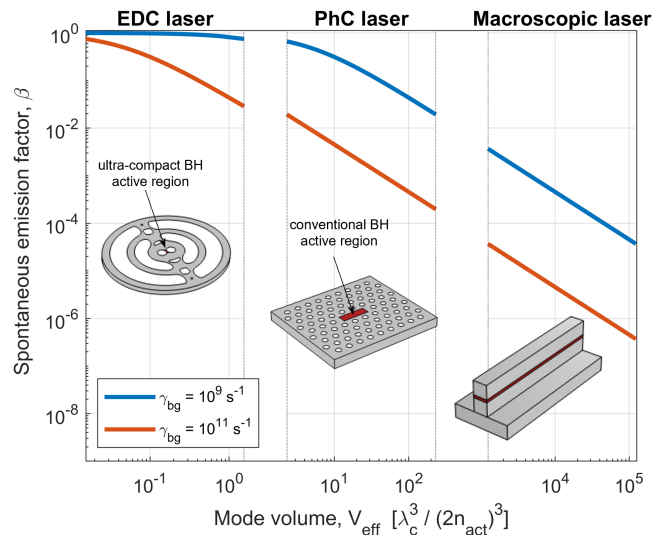


Figure 7. Spontaneous emission factor versus mode volume for a nanolaser with extreme dielectric confinement (EDC laser, left), a photonic crystal laser (PhC laser, center) and a conventional macroscopic laser (right). The spontaneous emission factor is shown for a value of the background decay rate equal to 10^9 s^{-1} (blue) and 10^{11} s^{-1} (red). The other parameters are the same as in Fig. 1. The number of emitters is fixed, while the mode volume varies with the optical confinement factor.

Therefore, it is clear that accurate estimates of the β -factor require relatively complex laser models. Nonetheless, Eq. 7 still retains a fundamental feature, that is the increase of the β -factor with decreasing mode vol-

ume for a given value of the background recombination rate. As an example, Fig. 7 illustrates the β -factor versus mode volume for an EDC laser (left), a PhC laser (center) and a macroscopic laser (right). The β -factor is shown for $\gamma_{bg} = 10^9 \text{ s}^{-1}$ (blue) and $\gamma_{bg} = 10^{11} \text{ s}^{-1}$ (red). The other parameters are the same as in Fig. 1. As already mentioned, the mode volume reflects, in each case (EDC, PhC and macroscopic laser), a total optical confinement ranging from 0.3% to 30%. PhC lasers exploiting the buried heterostructure (BH) technology already offer a small active region volume and a high optical confinement factor [69, 70]. Future cavity designs combining a BH active region and extreme dielectric confinement may further scale the active region volume while ensuring a high optical confinement factor. Such scaling may be accomplished without severely degrading the quality factor, as opposed to the case of plasmonic nanolasers [49, 104]. Therefore, EDC lasers may achieve higher values of spontaneous emission factor than macroscopic and even PhC lasers.

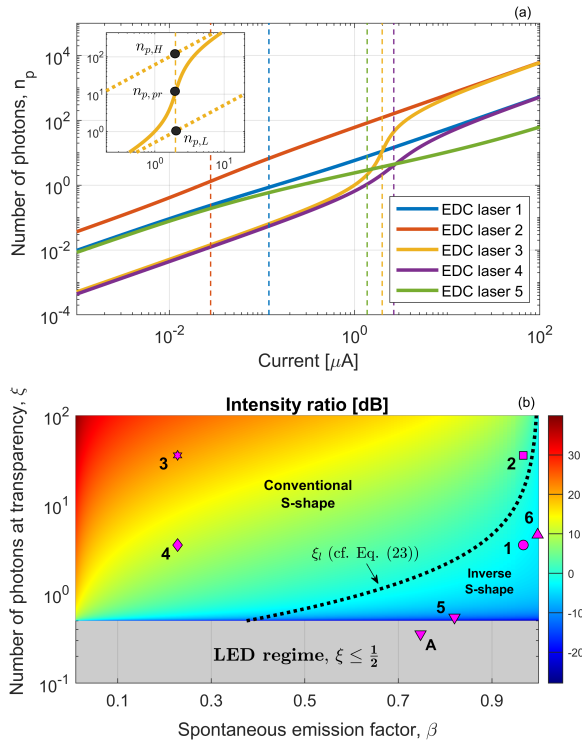


Figure 8. (a) Number of photons versus current for EDC lasers with parameters specified in Tab. I and leading to different values β and ξ . The vertical, dashed lines denote the threshold with photon recycling. The inset displays the LI characteristic (solid) of EDC laser 3 around the intensity jump and the asymptotes of the upper and lower branches (dotted). (b) Intensity ratio (cf. Eq. 20) in dB of the LI characteristic versus β and ξ . The markers correspond to the nanoscale devices in Tab. I. For the LI characteristic to be linear, β and ξ must follow the dotted line (cf. Eq. 23).

We shall now examine the role of the β -factor, β , and the number of photons at transparency, ξ , in shaping the LI characteristic. Fig. 8a shows the number of photons versus current for EDC laser 1 and other EDC lasers, with parameters specified in Tab. I. These parameters lead to different values of β and ξ . The vertical, dashed lines indicate the threshold current with photon recycling. The β -factor of EDC lasers 1 and 2 is close to 1 and the LI characteristic is almost linear. In EDC laser 3 and 4, instead, the β -factor drops to around 0.23 and a marked intensity jump shows up around threshold. This jump, however, is much more pronounced for EDC laser 3, which features a large value of ξ . Indeed, the intensity jump is determined by the pump injection efficiency, η , and the *effective* β -factor, β_{eff} , as shown below.

The inset of Fig. 8a zooms in on the LI characteristic of EDC laser 3 around threshold, displaying the asymptotes (dotted lines) and the threshold current with photon recycling (vertical line). By neglecting pump blocking and assuming $\gamma_r(2n_e - n_0)n_p \approx -\gamma_r n_0 n_p$ in the carrier and photon rate equations, we find the lower asymptote, $n_p = \beta_{\text{eff}}(I/q)/\gamma_c$. The upper asymptote, $n_p = \eta(I/q)/\gamma_c$, is found by neglecting the carrier recombination term compared to the net stimulated emission term in the carrier rate equation and assuming the carriers to be clamped. The upper and lower asymptotes at the threshold with photon recycling have a value of $n_{p,H} = (2\beta_{\text{eff}})^{-1}$ and $n_{p,L} = 1/(2\eta)$, respectively. Hence, to quantify the intensity jump, we introduce the intensity ratio

$$\frac{n_{p,H}}{n_{p,L}} = \frac{\eta}{\beta_{\text{eff}}} \quad (\text{intensity ratio}) \quad (20)$$

Despite having the same β -factor, EDC laser 3 and 4 feature different Q-factors. Moreover, β is close to, but not exactly equal to 1. Therefore, the larger value of ξ in EDC laser 3 results in a smaller β_{eff} (cf. Eq. 16), as well as in a larger η (cf. Eq. 13), ultimately implying a larger intensity ratio. Hence, we emphasize that the intensity jump of the LI characteristic is **not** a direct measure of the β -factor, as opposed to what commonly held (with some notable exceptions [32]).

From the LI characteristic, we also find the photon number at the threshold with photon recycling

$$n_{p,pr} = \frac{1}{2} \sqrt{\frac{1}{\eta\beta_{\text{eff}}}} \quad (21)$$

Interestingly, $n_{p,pr}$ is the geometric mean of $n_{p,H}$ and $n_{p,L}$. Furthermore, by comparing the expressions of I_{pr} and I_{tr} , one readily finds that the threshold with photon recycling is attained below transparency if

$$\xi\beta > 1 \quad (\text{intensity jump without inversion}) \quad (22)$$

This is the condition required for lasing without inversion [42], or, more precisely, intensity jump without inversion [32]. For example, EDC laser 1 fulfills Eq. 22, as evidenced by Fig. 4, where I_{pr} is seen to be smaller than I_{tr} .

Fig. 8b shows, in color scale, the intensity ratio versus β and ξ . The markers correspond to the nanolasers and the nanoLED in Tab. I. For values of ξ equal to or smaller than one-half, the intensity ratio is not defined, since the device operates as an LED. For larger values of ξ , it is seen that the intensity ratio may strongly depend on ξ , unless the β -factor is very close to one. The relation that β and ξ must fulfill for the LI characteristic to be linear is also shown (dotted line). This relation is found by requiring the intensity ratio to be equal to one, leading to

$$\xi_l = \frac{\beta + \sqrt{1 - \beta + \beta^2}}{4(1 - \beta)} \quad (\text{linear LI characteristic}) \quad (23)$$

In contrast to the common belief, we emphasize that a β -factor equal to one is **not** a necessary condition for a perfectly linear LI characteristic.

We also note that the LI characteristic shows the conventional S-shape on a double logarithmic scale if ξ is larger than ξ_l . For smaller values of ξ , instead, an *inverse* S-shape appears, with an intensity ratio smaller than 0 dB. In Fig. 8a, EDC laser 1 and, more markedly, EDC laser 5 feature LI characteristics with an inverse S-shape. Furthermore, as shown in Fig. 8b, the LI characteristic may evolve from the usual S-shape, to a straight line and finally to an inverse S-shape with increasing β -factor.

This behavior is consistent with the experimental results in [35], where the LI characteristic of a high- β nanolaser was measured at decreasing values of temperature. In [35], the phenomenon was explained as a complex interplay between zero-dimensional and two-dimensional gain contributions, depending on the temperature and the excitation power. Here, we point out that the effect naturally emerges from our rate equation model as γ_{bg} decreases for a given value of ξ . Experimentally, lower temperatures may suppress the non-radiative recombination, leading to lower values of γ_{bg} and larger values of β , with ξ being fixed. In practice, the emitter dephasing rate may actually decrease with decreasing temperature, leading to larger values of ξ . However, the transition from a conventional to an inverse S-shape would still occur as long as β increases sufficiently fast compared to ξ . It should be stressed that including pump blocking in the model is crucial to reproduce this behavior. If pump blocking is neglected ($\eta = 1$), the LI characteristic is only linear for $\beta = 1$ and the inverse S-shape does not appear under any circumstances.

To conclude this section, we point out that the re-

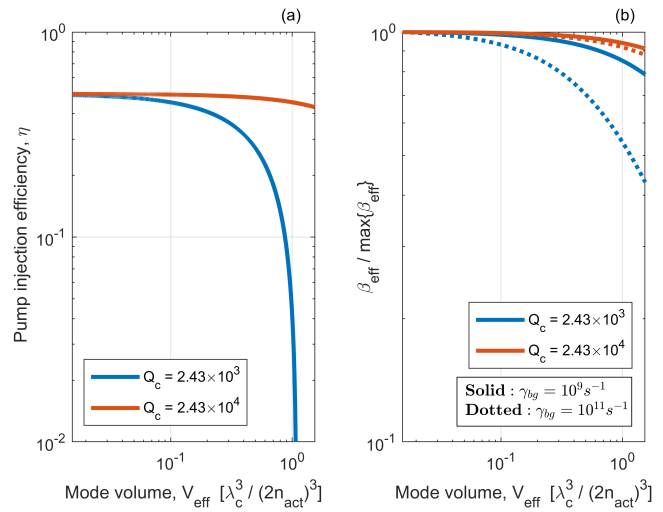


Figure 9. (a) Pump injection efficiency and (b) effective β -factor versus mode volume for the EDC laser in Fig. 1 (blue) and for an EDC laser with larger Q-factor (red), as indicated in the legend. In (b), the background decay rate is $\gamma_{bg} = 10^9 \text{ s}^{-1}$ (solid) and $\gamma_{bg} = 10^{11} \text{ s}^{-1}$ (dotted). In each case, the effective β -factor is normalized to the maximum value.

duction with decreasing mode volume of the threshold current with photon recycling (cf. Fig. 1) is mostly due to the larger pump injection efficiency, if the number of emitters is fixed. As an example, Fig. 9 shows (a) the pump injection efficiency (blue) and (b) the effective β -factor (blue, solid) versus mode volume for the EDC laser in Fig. 1. The effective β -factor is normalized to the maximum value. As the mode volume is reduced, the relative variation of the effective β -factor is negligible compared to the increase in the spontaneous emission rate per emitter, γ_r . Such an increase strongly reduces the number of carriers at the lasing threshold, n_{eth} , thereby limiting the impact of pump blocking, enhancing the pump injection efficiency, and ultimately decreasing the threshold current. However, the contribution of the β -factor to such a strong decrease is marginal, a conclusion which agrees with [72]. Indeed, a larger γ_r not only leads to a larger β -factor, but also to a larger number of photons at transparency. The two effects somehow balance out, resulting in a slight variation of the effective β -factor (cf. Eq. 16). Larger values of the background recombination rate (blue, dotted in Fig. 9b) obviously lead to a larger variation of β and thereby of β_{eff} , but the impact remains modest. Furthermore, larger values of the Q-factor naturally limit the variation of both η (red, in Fig. 9a) and β_{eff} (red, in Fig. 9b).

VI. OTHER THRESHOLD DEFINITIONS

Besides the classical threshold and the threshold with photon recycling, other threshold definitions have been proposed [32, 37, 39, 41, 43, 47], that we briefly review and compare in this section and the following.

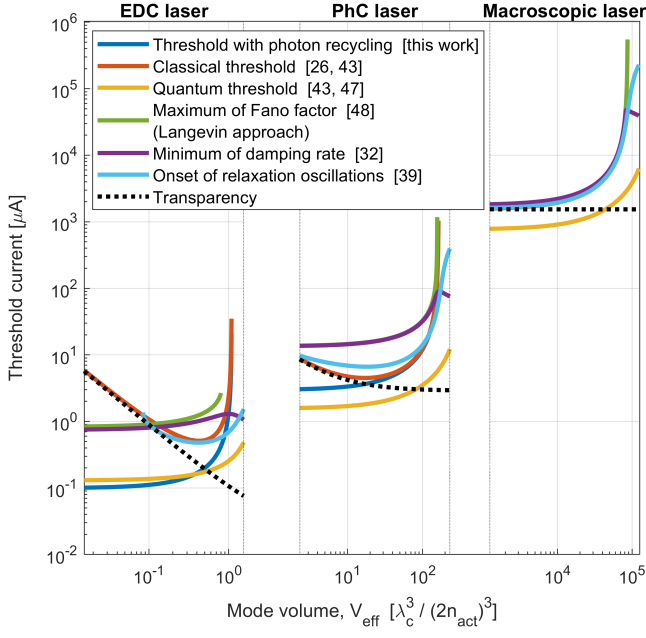


Figure 10. Threshold current versus mode volume for a nanolaser with extreme dielectric confinement (EDC laser, left), a photonic crystal laser (PhC laser, center) and a conventional macroscopic laser (right). Each color corresponds to a different threshold definition, as indicated in the legend. For the sake of comparison, the transparency current (dotted) is also shown. The parameters are the same as in Fig. 1. The number of emitters is fixed, while the mode volume varies with the optical confinement factor.

Fig. 10 shows the threshold current versus mode volume for an EDC laser (left), a PhC laser (center) and a conventional macroscopic laser (right), with the same parameters as in Fig. 1. Each color denotes a different threshold definition, as indicated in the legend. For the sake of comparison, the transparency current (dotted) is also included. For macroscopic lasers, all threshold definitions (except the quantum threshold, see below) approximately coincide [25, 39], provided that ξ is larger than one-half. Conversely, quantitative and qualitative differences gradually emerge among the various threshold definitions as the β -factor approaches unity, irrespective of the value of ξ . This is already observed for PhC lasers and, to a larger extent, for EDC lasers.

For PhC and EDC lasers, as already discussed in Sec. IV, the non-monotonic trend of the classical threshold current (red) stems from the counteracting variations of the transparency current and the pump in-

jection efficiency with decreasing mode volume. By contrast, the threshold current with photon recycling (blue) decreases and eventually saturates, due to an effective saturation of the carrier lifetime. A similar saturation is observed for other threshold definitions. We note that the classical threshold current in Eq. 12 differs from another expression, $\tilde{I}_{cl} = q\gamma_c/\beta$, reported elsewhere [25, 39]. In those works, stimulated absorption is not considered, assuming the lower lasing level to be quickly depopulated. As a result, the net stimulated emission term in the carrier and photon rate equations reduces to $\gamma_r n_e n_p$. Under this assumption, by neglecting pump blocking and applying the same procedure which leads to Eq. 12, one finds $\tilde{I}_{cl} = q\gamma_c/\beta$. However, a more realistic semiconductor laser model must include stimulated absorption [26, 32, 43]. Therefore, Eq. 12 better describes the classical threshold current of conventional semiconductor lasers.

The so-called quantum threshold [43, 47] (yellow line in Fig. 10) is attained when the stimulated emission, $\gamma_r n_e n_p$, equals the spontaneous emission into the lasing mode, $\gamma_r n_e$. Hence, the number of photons at the quantum threshold equals one. By utilizing this condition in Eq. 5 and Eq. 6, one finds the quantum threshold current

$$I_{qu} = \frac{q}{\eta_q} \frac{1}{3} \frac{\gamma_c}{\beta} [1 + 2\beta + 2\xi(1 - \beta)] \quad (\text{quantum threshold}) \quad (24)$$

where $\eta_q = \frac{2-1/(2\xi)}{3}$ and $\eta_q = 1$ with and without inclusion of pump blocking, respectively. For macroscopic lasers, the quantum threshold current and the classical threshold current approximately differ by a factor of two [43], unless the number of photons at transparency, ξ , tends to one-half. In this case, as discussed in Sec. IV, I_{cl} and I_{pr} diverge, since the maximum available gain cannot compensate for the cavity loss.

The Fano threshold (green line in Fig. 10) corresponds to the maximum of the Fano factor, F_F (see Eq. 8), as obtained from the Langevin approach. The Fano threshold definition originates from the enhancement of the intensity noise typically observed close to threshold [48]. In such a case, the peak of the Fano factor roughly marks the midpoint in the variation of the intensity correlation from a value of two to a value of one (cf. Fig. 5). This property often makes the Fano threshold an appealing indicator of the laser coherence. Unfortunately, the absence of a peak in the Fano factor as obtained from the Langevin approach does not necessarily imply the absence of lasing for EDC lasers. This is clearly seen from Fig. 11, showing the Fano factor (left) and the intensity correlation (right) of an EDC laser with mode volume, V_{eff} , equal to $0.9\lambda_c^3/(2n_{act})^3$. In such cases, more fundamental approaches to the quantum noise, such as stochastic simulations, may reveal a peak in the Fano factor (see Sec. VII) and thereby

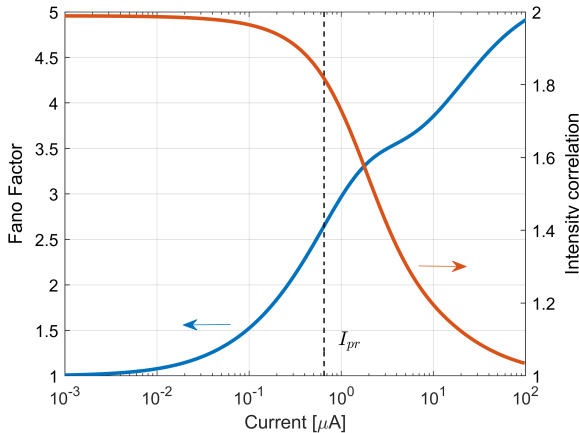


Figure 11. Fano factor (left) and intensity correlation (right) of an EDC laser with $V_{\text{eff}} = 0.9\lambda_c^3/(2n_{\text{act}})^3$. The other parameters are those of EDC laser 1 in Tab. I. The vertical, dashed line marks the threshold with photon recycling.

the existence of the Fano threshold. However, a general conclusion on the existence and location of such a peak cannot be drawn.

The minimum of the damping rate [32] and the onset of relaxation oscillations [39] have also been proposed as possible lasing threshold definitions. In Fig. 10, the corresponding currents are shown in purple and light blue, respectively. The damping rate is easily obtained from a small-signal analysis of Eq. 5 and Eq. 6. The eigenvalues, λ_{\pm} , of the linearized rate equation system are found by [26]

$$\lambda_{\pm} = -\frac{1}{2}\gamma \pm i\sqrt{\omega_R^2 - (\gamma/2)^2} \quad (25)$$

where γ is the damping rate and ω_R is the relaxation resonance frequency. Relaxation oscillations exist if the imaginary part of the eigenvalues is nonzero [39]. However, we note that the presence or absence of relaxation oscillations is not generally sufficient to confirm or rule out lasing. For instance, it is well known that lasers of class-A [105], characterized by $\gamma_r + \gamma_{bg} \gg \gamma_c$, do not show relaxation oscillations. This is the reason why, for mode volumes smaller than a specific value, no threshold is found marking the onset of relaxation oscillations in EDC lasers. We also note that the minimum of the damping rate approximately corresponds, in a wide range of mode volumes, to the maximum of the Fano factor, as already noted for PhC lasers [32]. However, the two thresholds are not generally equivalent, especially for EDC lasers.

Besides the above observations, we emphasize that if a lasing threshold exists, the photon statistics must asymptotically approach a Poisson process as the current increases above threshold. This is a fundamental

reliability test that any threshold definition should pass to be general. As we show below, neither the quantum threshold, nor the definitions based on the damping rate or the relaxation oscillations, necessarily pass such a test.

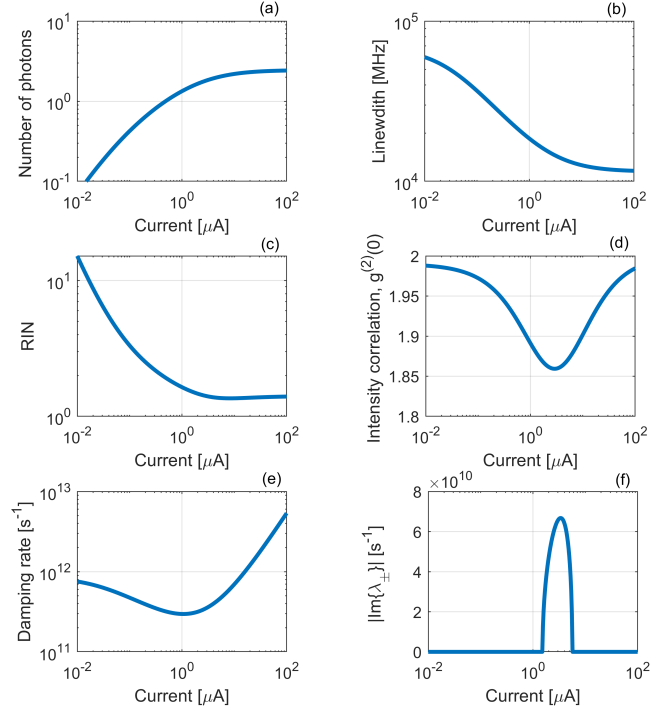


Figure 12. Current dependence of key characteristics of nanoLED A with parameters summarized in Tab. I. (a) Photon number, (b) modified Schawlow-Townes linewidth, (c) relative intensity noise, (d) intensity correlation, (e) damping rate and (f) absolute value of the imaginary part of the rate equations eigenvalues.

In Fig. 12, we consider the input-output and small-signal characteristics of nanoLED A, with parameters summarized in Tab. I. These parameters lead to a value of ξ smaller than one-half, which makes the classical threshold and the threshold with photon recycling unattainable. On the contrary, the quantum threshold exists, as evident from Fig. 12a, where the number of photons is seen to reach and overcome a value of one. The linewidth somewhat narrows, as displayed by Fig. 8b, but the photon number saturates at current values beyond the quantum threshold. Correspondingly, the photon statistics tends to the limit of thermal light. This is clearly seen from Fig. 12c and Fig. 12d, showing the relative intensity noise and the intensity correlation, respectively. This example suggests that neither the quantum threshold nor the linewidth narrowing are reliable indicators of lasing, as also noted in [35]. Fig. 12e and Fig. 12f, showing, respectively, the damping rate and the imaginary part of the eigenvalues,

would also suggest the existence of lasing. Nonetheless, as discussed above, coherent laser light is out of reach, irrespective of the pumping level.

It should be mentioned that the onset of lasing in the thermodynamic limit is marked by the appearance of a bifurcation [39]. Therefore, it has been argued that the emergence of the coherent optical field from a bifurcation is the primary and sole lasing threshold definition, a so called bifurcation threshold [39]. However, rate equation models, that include spontaneous emission in the lasing mode, do not feature a bifurcation [39] and one cannot identify, therefore, a bifurcation threshold outside the thermodynamic limit. A recent work [37], at the center of a vivid debate [38–40], has proposed a laser model ostensibly featuring a bifurcation all the way from the thermodynamic limit to the case of $\beta = 1$. Based on this model, an expression for the pumping rate at the bifurcation threshold has been reported [37]. Setting aside considerations on the laser model, we briefly comment on this threshold expression.

Consistently with Sec. III, we assume the emitters in resonance with the lasing mode and consider the practically relevant case of the good-cavity limit, $\gamma_2 \gg \gamma_c$. Under these assumptions, the pumping rate per emitter at threshold reported in [37] leads to a threshold current given by

$$I_b = \frac{q}{\eta} \frac{\gamma_c}{2} (2\xi + 1) \left(\frac{1}{\beta} + \frac{\gamma_2}{\gamma_c} \right) \quad (\text{bifurcation threshold}) \quad (26)$$

We note that the existence of a minimum number of emitters to achieve lasing [37] is embedded in the pump injection efficiency, η , and stems from considering a finite maximum gain, $n_0\gamma_r$. For macroscopic lasers, assuming ξ larger than one-half, I_b only coincides with the other threshold definitions if β^{-1} is much larger than γ_2/γ_c , which is not necessarily the case. For EDC lasers, considering $\beta \approx 1$ and ξ much larger than one-half, one finds $I_b \approx qn_0\gamma_r\gamma_2/\gamma_c$. In such a case, I_b increases with decreasing mode volume, like the classical threshold current. However, I_b also increases with increasing Q-factor, which is counter-intuitive and calls for further investigations.

VII. PHOTON DISTRIBUTIONS AND STOCHASTIC THRESHOLD

In the previous sections, we used the Langevin approach [26] to model the quantum noise. However, this approach may break down for very few emitters, in which case stochastic approaches [44, 86] are more accurate. In this section, we analyze the transition to lasing in EDC lasers by applying a recently developed stochastic approach [45], briefly explained in Sec. III.

Importantly, the stochastic approach gives access

to the probability distribution of the photon number. Therefore, we can also explore another definition of lasing threshold, the so-called *stochastic threshold*, as we name it in the following. At this threshold, the probabilities of having zero photons and one photon inside the cavity are equal [41]. The fact that such a balance is fulfilled at the threshold of macroscopic lasers [25, 106] motivates the definition. Still, it does not ensure that the concept also applies at the nanoscale. With the aid of a density-matrix approach, the extension of the stochastic threshold to nanolasers has been argued for [41]. Here, we investigate the stochastic threshold by utilizing the stochastic approach.

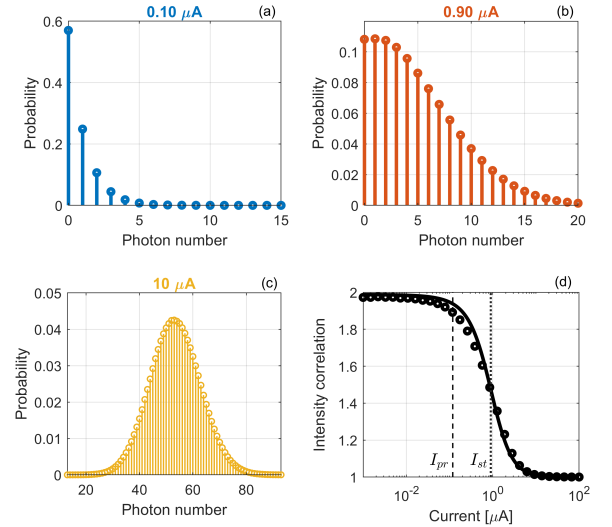


Figure 13. Probability distributions of the intracavity photons for EDC laser 1 in Tab. I at (a) $0.10 \mu\text{A}$, (b) $0.90 \mu\text{A}$ and (c) $10 \mu\text{A}$. The current value in (b) marks the stochastic threshold. At this threshold, the probabilities of having zero photons and one photon inside the cavity are equal. (d) Intensity correlation of EDC laser 1 versus current as obtained from stochastic simulations (markers) and Langevin approach (solid line). The vertical lines mark the threshold with photon recycling, I_{pr} (dashed), and the stochastic threshold, I_{st} (dotted).

We shall first reconsider the case of EDC laser 1, with parameters summarized in Tab. I. Fig. 13 shows the probability distributions of the intracavity photon number at a current (a) well below, (b) corresponding to and (c) well above the stochastic threshold. The probability distribution is obtained from the time-resolved photon number as the fraction of the total simulation time spent with a given value of the photon number. Well above the stochastic threshold, a Poisson distribution is approached, which indicates lasing. This is consistent with Fig. 13d, showing the intensity correlation versus current. Results obtained from the Langevin approach (lines) and the stochastic approach (markers) match pretty well. Higher accuracy is expected from

the stochastic approach, which does not rely on a small-signal approximation [46].

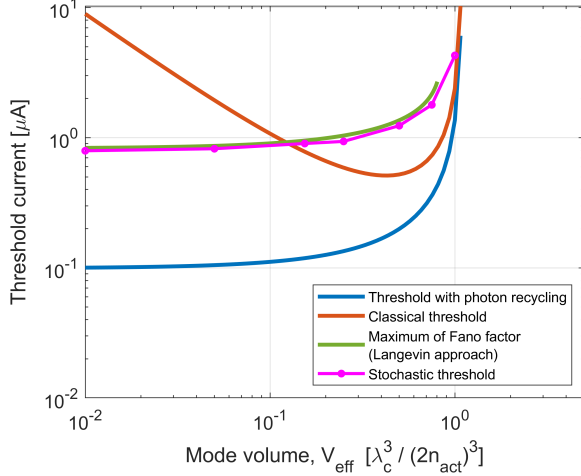


Figure 14. Threshold current versus mode volume for an EDC laser, with the same parameters as in Fig. 1. Each color denotes a different threshold definition, as specified in the legend. The number of emitters is fixed, while the mode volume varies with the optical confinement factor.

Fig. 14 shows the threshold current versus mode volume, including the threshold with photon recycling (blue), the classical threshold (red), the Fano threshold from the Langevin approach (green) and the stochastic threshold (pink). The stochastic threshold current, I_{st} , is computed numerically from the probability distribution of the intracavity photon number, with each marker corresponding to a given value of mode volume. The threshold current with photon recycling, I_{pr} , scales similarly to I_{st} , even though the absolute values generally differ. Importantly, the two thresholds tend to match as the mode volume increases and pump blocking gradually prevents the possibility of lasing. Interestingly, the stochastic threshold almost coincides with the Fano threshold. This is not, though, a general feature, as the next example shows.

To highlight the difference between the Langevin and the stochastic approaches, we consider the case of a single-emitter nanolaser. Fig. 15 shows (a) the intensity correlation and (b) the Fano factor versus current for EDC laser 6 in Tab. I (red). Two other EDC lasers are also considered, with a smaller (blue) and a larger (yellow) mode volume, as indicated in the legend. The larger Q-factor ($Q_c \approx 2.3 \times 10^4$) compared to EDC laser 1 leads to threshold current values low enough that including pump broadening (see Sec. III) would have a negligible impact. The vertical, dashed lines denote the threshold with photon recycling. As the current increases from below to above threshold, the stochastic approach (markers) successfully captures the change in the photon statistics from anti-bunched

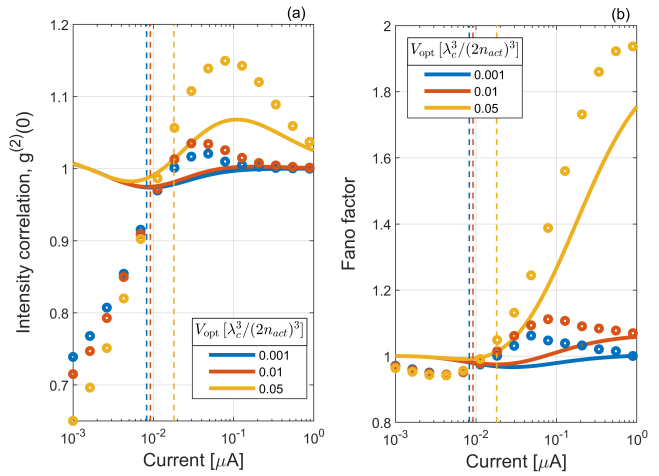


Figure 15. (a) Intensity correlation and (b) Fano factor versus current for single-emitter nanolasers: EDC laser 6 in Tab. I (red) and two other EDC lasers, with a smaller (blue) and a larger (yellow) mode volume, as indicated in the legend. The other parameters are those of EDC laser 6. Solid lines and markers correspond to the Langevin approach and the stochastic approach, respectively. The vertical, dashed lines indicate the threshold with photon recycling.

$(g^{(2)}(0) < 1)$ to bunched ($g^{(2)}(0) > 1$) and finally coherent light ($g^{(2)}(0) \approx 1$), as expected for a single-emitter nanolaser [46, 64]. On the other hand, results from the Langevin approach (solid lines) are seen to be qualitatively wrong. At larger current values (not shown in the figures), both approaches would reveal a further transition to thermal light if pump broadening were included [46].

Interestingly, the threshold with photon recycling marks, with good approximation, the transition from the non-classical regime of anti-bunched light to the classical photon bunching regime which precedes lasing, as confirmed by full quantum simulations [46]. In this sense, the threshold with photon recycling does mark the onset of the change of the photon statistics toward coherent laser light, all the way from the macro-scale (see Sec. IV) to the extreme case of a single emitter.

The variation with mode volume of the threshold current is illustrated in Fig. 16, showing the threshold with photon recycling (blue), the classical threshold (red) and the stochastic threshold (pink). The stochastic threshold and the threshold with photon recycling are again seen to scale similarly and to gradually match as pump blocking becomes important. Note that the Fano factor computed by the Langevin approach features no peak (cf. Fig. 15b). Hence, Fig. 16 does not include the Fano threshold. On the other hand, depending on the mode volume, the stochastic approach may bring out a peak in the Fano factor. In such cases (blue and red markers in Fig. 15b), the stochastic approach indicates,

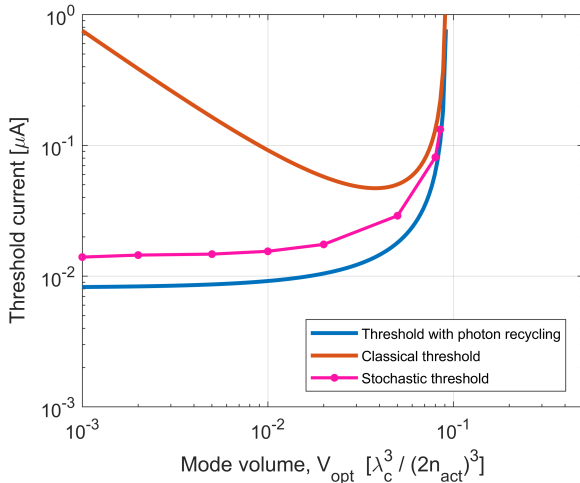


Figure 16. Threshold current versus mode volume for a single-emitter EDC laser. Other than the mode volume, the parameters are those of EDC laser 6 in Tab. I. Each color denotes a different threshold definition, as specified in the legend.

unlike the Langevin approach, that the Fano threshold does exist.

A systematic investigation of the Fano threshold as obtained from stochastic simulations is beyond the scope of this article. Nonetheless, here we emphasize that the Fano threshold and the stochastic threshold are not generally equivalent, despite what Fig. 14 might suggest. In fact, the Fano threshold current emerging from the stochastic approach (cf. Fig. 15b) is found to be quite different from the stochastic threshold current (cf. Fig. 16).

VIII. CONCLUSIONS

Emerging dielectric cavities with deep sub-wavelength optical confinement (so-called extreme dielectric confinement, EDC) [13–16, 18] are an attractive platform for ultra-compact and energy-efficient nanolasers. EDC cavities may strongly enhance the spontaneous emission rate per emitter, γ_r , thus featuring a near-unity spontaneous emission factor, β . Cavity designs combining a compact active region [69, 70] or a single-emitter [46, 64] with extreme dielectric confinement may culminate in EDC lasers featuring an ultra-low threshold current.

The classical approach [26] to computing the threshold current shows its limits in EDC lasers, where most of the spontaneously emitted photons are funneled into the lasing mode and are more likely to be re-absorbed than decaying. In this article, we have proposed, derived, and thoroughly discussed a new threshold defini-

tion, the so-called *threshold with photon recycling*. The concept arises from a simple observation, but with considerable physical implications: the number of carriers below threshold is accurately estimated by neglecting the stimulated emission, but retaining the stimulated absorption (cf. Fig. 3). The new threshold, Eq. 17, generalizes the classical balance between gain and loss by incorporating the physics of photon recycling [42]. It reduces to the classical threshold current, Eq. 12, in the limit of $\beta \ll 1$, whereas quantitative, as well as qualitative differences emerge for $\beta \rightarrow 1$ (cf. Fig. 1). The merits of the threshold with photon recycling are:

- Consistently marking the onset of the transition in the second-order intensity correlation, $g^{(2)}(0)$, toward coherent laser light, irrespective of the laser size and down to the case of a single emitter.
- Pointing out that a transition to lasing does exist even in the case of a perfectly linear (so-called "thresholdless") light-current characteristic.
- Identifying the onset of the transition based on physical, rather than empirical arguments.
- Marking the inflection point of the light-current characteristic if the latter features an intensity jump.
- Reliably distinguishing between lasers and LEDs.

Importantly, we have clarified that some threshold currents, such as the quantum threshold [47], are unreliable indicators of lasing (cf. Fig. 12), and others [37] may scale, for EDC lasers, in a dubious manner. Stochastic simulations reveal that the stochastic threshold, recently proposed [41], scales with the mode volume in a similar fashion as the threshold with photon recycling.

Furthermore, we have shown that a linear light-current characteristic does **not** require $\beta = 1$ if one accounts for the finite number of electronic states that may contribute to lasing (cf. Fig. 8). This is important to consider in single-mode nanolasers, such as EDC lasers, even in the presence of extended active media. This observation contrasts with common belief, but appears to agree with experimental results [35].

Our investigations provide a systematic overview of the many different threshold definitions for micro- and nanolasers (cf. Fig. 10) that have emerged during a long and vivid debate [4, 25, 27, 32, 37–41, 43, 47–49, 72]. Besides shedding light on the fundamental question of the transition to lasing, these findings may guide future nanolaser designs. Inclusion of the phase noise, currently neglected, in the stochastic simulation scheme could further elucidate the role of the threshold with photon recycling.

IX. APPENDIX A: SPONTANEOUS EMISSION RATE PER Emitter

In this section, we formally derive the spontaneous emission rate per emitter, γ_r . Importantly, we discuss the mode volume, V_p , which enters the expression of γ_r (cf. (1)) in the case of a single emitter and the more general situation of an extended semiconductor active medium. We restrict the analysis to the weak-coupling [65, 107] limit, since rate equations are not valid in the strong-coupling regime.

From Fermi's golden rule, the spontaneous emission rate of an emitter embedded in an optical cavity is proportional to the local **photonic density of states** (LDOS) [108]. This represents the density of optical modes, per unit frequency and unit volume, at the position of the emitter. The calculation of the LDOS is a subtle issue, which essentially amounts to computing the so-called *quasi-normal* modes (QNMs) [109]. Also known as leaky modes [110], QNMs are solutions of time-harmonic, source-free Maxwell's equations with radiation boundary conditions. Their frequencies are complex, with the imaginary part being the damping rate of the mode. Importantly, the boundary conditions ensure that energy leaks away from the resonator, but they also imply that the field distributions diverge in space at sufficiently large distances from the cavity. This divergence raises the crucial question of the QNMs normalization [111–113], which is at the core of a rigorous definition of the optical mode volume [19, 20, 66, 67].

A. Single emitter

We start by considering a single emitter, e.g. a quantum dot, placed inside the cavity at the position \mathbf{r}_e and described as an ideal two-level system. For an ideal, lossless cavity, Maxwell's equations may be reduced to an *hermitian* eigenvalue problem [114], implying that the eigenfrequencies are real and the eigenmodes constitute a complete orthonormal basis - the so-called *normal* modes. In the presence of losses, the eigenvalue problem becomes non-hermitian [115]. However, if the losses are small, the field distributions and the real part of the eigenfrequencies are unchanged to the first order, while the resonances are broadened with a Lorentzian lineshape. Under these assumptions, the LDOS reads [66]

$$\rho_{opt}(\mathbf{r}_e, \omega) = \sum_m \frac{1}{V_{opt,m}(\mathbf{r}_e)} \left[\frac{1}{\pi} \frac{\gamma_{c_m}/2}{(\omega - \omega_{c_m})^2 + (\gamma_{c_m}/2)^2} \right] \quad (27)$$

where the summation is over the modes of the cavity. The resonance frequency and damping rate of the m -th mode are ω_{c_m} and $\gamma_{c_m}/2$, respectively. The mode

volume, $V_{opt,m}(\mathbf{r}_e)$, is defined by

$$\frac{1}{V_{opt,m}(\mathbf{r}_e)} = \frac{\epsilon_0 n^2(\mathbf{r}_e) |\hat{\mathbf{d}}_e \cdot \mathbf{E}_m(\mathbf{r}_e)|^2}{\int_V \epsilon_0 n^2(\mathbf{r}) |\mathbf{E}_m(\mathbf{r})|^2 d^3 \mathbf{r}} \quad (28)$$

Here, \mathbf{E}_m is the electric field of the m -th mode and $n^2(\mathbf{r}_e)$ is the refractive index at the position of the emitter. The emitter dipole moment is denoted by $\mathbf{d}_e = d_e \hat{\mathbf{d}}_e$, with $\hat{\mathbf{d}}_e$ being the unit vector which represents the orientation of the dipole. The integration volume, V , deserves some comments.

In the far field of the resonator, the amplitude of the m -th mode grows like $\exp[\gamma_{c_m} r / (2c)] / r$ [19], with $r = |\mathbf{r}|$ being the amplitude of the position vector and c being the light speed. Therefore, the integral at the denominator of (28) diverges as the integration volume tends to infinity. However, the exponential growth of the mode starts only being effective at a distance $r \approx Q_m \lambda_m / \pi$ from the cavity, with $Q_m = \omega_{c_m} / \gamma_{c_m}$ being the quality factor of the mode and λ_m the resonant wavelength. Consequently, if the quality factor is high enough, the mode volume can be computed, for all practical purposes, by using (28). The integration volume can be truncated more or less arbitrarily if enclosing the physical volume of the cavity with a margin of a few wavelengths. The approach is reasonable for the lasing mode of nanolasers with extreme dielectric confinement, but not, e.g., for plasmonic nanolasers [49, 104], where substantial ohmic losses strongly limit the quality factor. In this case, leakage cannot be viewed as a small perturbation and generalized versions [19, 20, 66, 67] of (27) and (28) should be employed.

Since we are interested in the spontaneous emission rate into the lasing mode, we must isolate this mode from (27). By taking into account the homogeneous broadening of the emitter, Fermi's Golden rule reads [65]

$$\bar{r}_{sp_0}(\mathbf{r}_e, E_{21}) = \frac{2\pi}{\hbar^2} d_e^2 \int \frac{\hbar\omega}{2\epsilon_0 n^2(\mathbf{r}_e)} \rho_c(\mathbf{r}_e, \omega) L(\hbar\omega - E_{21}) d\omega \quad (29)$$

Here, $\rho_c(\mathbf{r}_e, \omega) = \frac{1}{V_{opt}(\mathbf{r}_e)} \left[\frac{1}{\pi} \frac{\gamma_c/2}{(\omega - \omega_c)^2 + (\gamma_c/2)^2} \right]$ is the LDOS of the lasing mode (for simplicity, we have dropped the subscript m) and

$$L(\hbar\omega - E_{21}) = \frac{1}{\pi} \frac{\hbar\gamma_2/2}{(\hbar\omega - E_{21})^2 + (\hbar\gamma_2/2)^2} \quad (30)$$

is the **homogeneous broadening** lineshape. This lineshape effectively describes the broadening of the emitter transition energy around a central value, E_{21} , due to various decoherence processes.

In practice, (29) can be simplified by noting that the term $\hbar\omega$ under the integral is slowly varying as compared to the LDOS. Thus, we may assume $\hbar\omega \approx \hbar\omega_c$

and bring this term outside of the integral. Then, (29) becomes $\bar{r}_{sp_0}(\mathbf{r}_e, E_{21}) \approx E_{vf}^2(\mathbf{r}_e) \bar{r}_{sp_0}(E_{21})$, where

$$E_{vf}^2(\mathbf{r}_e) = \frac{\hbar\omega_c}{2\epsilon_0 n^2(\mathbf{r}_e) V_{opt}(\mathbf{r}_e)} \quad (31)$$

is the square of the vacuum-field amplitude of the lasing mode [65] and

$$\bar{r}_{sp_0}(E_{21}) = \frac{2d_e^2}{\hbar^2} \frac{\frac{\gamma_c + \gamma_2}{2}}{\left(\omega_c - \frac{E_{21}}{\hbar}\right)^2 + \left(\frac{\gamma_c + \gamma_2}{2}\right)^2} \quad (32)$$

stems from the convolution of the homogeneous broadening lineshape and the LDOS of the lasing mode [107].

For our purposes, (32) should be taken in the so-called **good-cavity limit**, $\gamma_2 \gg \gamma_c$, where the rate equations are valid. Furthermore, the good-cavity limit is the relevant scenario for emitters working at room temperature, where the emitter dephasing time is on the order of a few tens of femtoseconds [89]. By further assuming that the emitter is in resonance with the lasing mode, we find

$$\bar{r}_{sp_0}(\mathbf{r}_e) = \frac{2d_e^2}{\hbar\epsilon_0 n^2(\mathbf{r}_e)} \frac{\omega_c}{\gamma_2} \frac{1}{V_{opt}(\mathbf{r}_e)} \quad (33)$$

which coincides with (1) for $V_p = V_{opt}(\mathbf{r}_e)$. We note that in the opposite limit, $\gamma_2 \ll \gamma_c$ (bad-cavity limit), we would find the usual expression [65, 116] for the Purcell factor.

B. Extended active medium

We now consider an extended semiconductor active medium, such as an active region with multiple quantum well or quantum dot layers. The active medium consists of an ensemble of emitters, which give rise to a band structure of energy levels. This is the situation encountered in conventional semiconductor lasers. In this case, the spontaneous emission rate into the lasing mode reads

$$r_{sp_0} = \int \int \bar{r}_{sp_0}(\mathbf{r}_e, E_{21}) \rho_{elec}(E_{21}) f_e(E_2) f_h(E_1) dE_{21} d^3 \mathbf{r}_e \quad (34)$$

Here, $\rho_{elec}(E_{21})$ is the so-called reduced **electronic density of states** (DOS) [26, 117], which represents the density of electron-hole transitions (electronic states) per unit transition energy and per unit active region volume. The electronic DOS reflects the **inhomogeneous broadening** of the transition energy, $E_{21} = E_2 - E_1$, as determined by the band structure of the active medium. Here, E_2 , is the energy of an electron in the conduction band, while E_1 is the energy of a hole in the valence band. Both E_2 and E_1

are uniquely determined by E_{21} , due to conservation of energy and momentum [26, 117]. For a spontaneous emission event to happen, an electron-hole pair should be present. Hence, the product of the electron occupation probability, $f_e(E_2)$, and hole occupation probability, $f_h(E_1)$, appears in (34). Since the intraband dynamics is neglected, the occupation probabilities are Fermi-Dirac distributions. Implicitly, both probabilities were assumed to be unitary in (29). Furthermore, we note that diffusion effects are expected to even out the distribution of carriers throughout the active region. Therefore, the occupation probabilities do not depend on space. Finally, we note that the integration with respect to the emitter position, \mathbf{r}_e , is over the physical volume of the active region, V_{act} , where the emitters are spatially distributed.

By using the expression of the vacuum field, (34) becomes

$$r_{sp_0} = \frac{\hbar\omega_c}{2\epsilon_0 n_{act}^2} \Gamma \int \bar{r}_{sp_0}(E_{21}) \rho_{elec}(E_{21}) f_e(E_2) f_h(E_1) dE_{21} \quad (35)$$

where the optical confinement factor, Γ , reads

$$\Gamma = \frac{\int_{V_{act}} \epsilon_0 n_{act}^2 \left| \hat{\mathbf{d}}_e \cdot \mathbf{E}(\mathbf{r}_e) \right|^2 d^3 \mathbf{r}_e}{\int_V \epsilon_0 n^2(\mathbf{r}) \left| \mathbf{E}(\mathbf{r}) \right|^2 d^3 \mathbf{r}} \quad (36)$$

Here, the active region refractive index, n_{act} , is the refractive index at the emitter position, assumed to be uniform over the active region volume. The orientation of the dipole at position \mathbf{r}_e is formally retained in (36). In practice, we may assume $|\hat{\mathbf{d}}_e \cdot \mathbf{E}(\mathbf{r}_e)|^2 \approx |\mathbf{E}(\mathbf{r}_e)|^2$ and account for any non-perfect alignment between electric field and dipoles via an effective reduction of the amplitude of the dipole moment. For quantum well active media, this reduction depends on the polarization of the electric field, owing to the particular symmetries of the conduction and valence band Bloch functions [26]. With these considerations in mind, (36) is the usual expression [117] for the optical confinement factor of semiconductor lasers theory. We note that the amplitude of the dipole moment, d_e , in (35) is formally embedded into $\bar{r}_{sp_0}(E_{21})$, but its dependence on the transition energy can be often neglected [26]. The connection with the transition matrix element, $|M_T|^2$, is given by $d_e^2 = q^2 |M_T|^2 / (m_0 \omega_c)^2$ [26], where m_0 is the vacuum electron mass.

In general, (35) cannot be further simplified and it is necessary to proceed numerically. In particular, the occupation probabilities are nonlinear functions of the injection level via the quasi-Fermi levels of electrons and holes. The standard approach requires the active region to be charge neutral, implying that the total number of electrons and holes has to be the same. Thus, both quasi-Fermi levels are linked to a given number of carriers, with a relation depending on the type of active

material (bulk, quantum well, etc.) - for details, see [26, 117]. At a given number of carriers, the quasi-Fermi levels are found and one needs to solve the integral in (35) with respect to the transition energy. By iterating this procedure, the spontaneous emission rate into the lasing mode is found as a function of the number of carriers. Incidentally, we note that by proper modification of (35) and applying the same procedure, one may also find the stimulated emission rate and *total* spontaneous emission rate. Then, the rate equations of photons and carriers may be solved in a purely numerical fashion [63, 71, 81].

Here, consistently with Sec. III, we pursue a simpler strategy and assume a linear dependence of spontaneous and stimulated emission on the number of carriers. This approximation is reasonable if the injection level is not much higher than the transparency condition [26, 117] and it is widely employed in the literature [70, 78, 79]. To single out the spontaneous emission rate per emitter, γ_r , from (35), we assume the occupation probabilities to be unitary, corresponding to the ideal scenario of full inversion. Under these conditions, the spontaneous emission rate into the lasing mode equals $\gamma_r n_0$, with n_0 being the total number of carriers. We note that the linear approximation would not hold at injection levels high enough to reach full inversion and that, in practice, the onset of lasing and other phenomena, such as temperature increase, would preclude the full inversion anyway. Therefore, this approach should be interpreted as an extrapolation procedure.

We start by considering a quantum dot active medium with negligible inhomogeneous broadening. In this case, the electronic DOS reads $\rho_{elec}(E_{21}) = (2n_{QD}/V_{act})\delta(E_{21} - E_s)$ [71], where n_{QD} is the number of quantum dots, V_{act} is the total volume of the quantum dots and E_s is the energy of the ground state transition. Higher-order transitions are neglected. The factor of 2 takes into account the spin degeneracy, implying $n_0 = 2n_{QD}$. By requiring $r_{sp_0} = \gamma_r n_0$, we find

$$\gamma_r = \frac{2d_e^2}{\hbar\epsilon_0 n_{act}^2} \frac{\omega_c}{\gamma_2} \frac{\Gamma}{V_{act}} \quad (37)$$

For simplicity, we have assumed the ground state transition of the quantum dots to be in resonance with the lasing mode. Any detuning would amount to quantitative, but not qualitative changes. Furthermore, consistently with (33), we have considered the good-cavity limit. Importantly, (37) shows that γ_r scales with an *effective* mode volume, $V_{eff} = V_{act}/\Gamma$.

In practice, the epitaxial semiconductor growth process leads to unavoidable variations in the physical size of the quantum dots and the formation of a wetting layer [118]. By neglecting all energy transitions higher than the ground state, the electronic DOS is usually modeled by a Gaussian distribution [26, 71], with an

average ground state energy, E_s , and a standard deviation, σ . Hence, the integration over the transition energies reduces to a convolution between a Gaussian distribution and a Lorentzian function, reflecting inhomogeneous and homogeneous broadening, respectively. Unfortunately, this convolution can only be computed numerically. However, it is easy to realize that the inhomogeneous broadening would effectively increase the dephasing rate, γ_2 , in (37). One may approximate the Gaussian distribution with a Lorentzian function having the same full width at half-maximum, $2\sigma\sqrt{2\ln(2)}$. By assuming, as done above, $E_s = \hbar\omega_c$, one would find

$$\gamma_r = \frac{2d_e^2}{\hbar\epsilon_0 n_{act}^2} \frac{\omega_c}{(\gamma_2 + 2\sigma\sqrt{2\ln(2)}/\hbar)} \frac{\Gamma}{V_{act}} \quad (38)$$

Hence, the inhomogeneous broadening would amount to quantitative, but not qualitative changes in the expression of γ_r .

Finally, we consider a quantum well active medium. In this case, the reduced electronic DOS is a staircase function [26], reflecting the presence of multiple subbands. Hence, the integration over the transition energies generally depends in a nontrivial manner on the energy difference between the subbands edges and the relative position of the lasing mode frequency. However, we may attempt a rough estimate by assuming the lasing mode to be in resonance with the ground state and neglecting higher-order subbands. Hence, the reduced electronic DOS reads $\rho_{elec} = m_r/(d_{QW}\pi\hbar^2)$, where m_r is the reduced effective mass and d_{QW} the thickness of any of the quantum well layers. By using (35) under the assumption of full inversion and the good-cavity limit, we find

$$r_{sp_0} = \gamma_r n_0 = \left(\frac{2d_e^2}{\hbar\epsilon_0 n_{act}^2} \frac{\omega_c}{\gamma_2} \frac{\Gamma}{V_{act}} \right) \left(\frac{m_r \gamma_2 V_{act}}{4\hbar d_{QW}} \right) \quad (39)$$

from which we may identify an effective number of emitters, $n_0 = (m_r \gamma_2 V_{act})/(4\hbar d_{QW})$, and an expression for γ_r formally identical to (37). The transparency carrier density corresponding to the effective number of emitters would be $N_{tr} = n_0/(2V_{act})$, which is not far from typical values [26] reported in the literature. Here, V_{act} is the volume including all the quantum well layers.

In conclusion, the spontaneous emission rate per emitter, γ_r , is given by (37) for an extended active medium. Consistently with the conventional theory of semiconductor lasers [26, 117] and previous works on nanolasers [63, 71], we find γ_r to be inversely proportional to an effective mode volume. This mode volume is defined by the ratio between the physical volume of the active region, V_{act} , and the optical confinement factor, Γ , which is the fraction of electric energy stored within V_{act} . In the case of a quantum dot active medium, V_{act} is the total volume of the quantum dots, that is the sum of the volumes of every single dot. We note that

the relation between γ_r and the differential gain [26], g_N , is

$$\gamma_r = \frac{v_g g_N}{2V_{\text{eff}}} \quad (40)$$

where v_g is a group velocity reflecting material, but not structural dispersion [44].

As opposed to conventional laser designs, designs based on extreme dielectric confinement (EDC) [13–16, 18] would enable dramatic scaling of the active region volume, without compromising the optical confinement factor. Incidentally, we note that a unitary optical confinement factor may be achieved by combining a bulk active material with an EDC design. In this case, γ_r would scale with the inverse of the active region volume.

X. APPENDIX B: PHOTON VARIANCE FROM THE LANGEVIN APPROACH

From a small-signal analysis of (5) and (6) with added Langevin noise forces [26], we compute the fluctuation of the photon number around the average and subsequently the power spectral density of the photon number. By integrating this spectral density over all frequencies, we obtain the variance of the photon number

[44]

$$\langle \Delta n_p^2 \rangle = \frac{1}{\gamma} \left[\left(1 + \frac{\Gamma_{ee}^2}{\omega_R^2} \right) D_{pp} + \frac{\Gamma_{pe}^2}{\omega_R^2} D_{ee} + \frac{2\Gamma_{pe}\Gamma_{ee}}{\omega_R^2} D_{pe} \right] \quad (41)$$

Here, $\Gamma_{ee} = \gamma_p + \gamma_t + 2\gamma_r n_p$, $\Gamma_{ep} = \gamma_r(2n_e - n_0)$, $\Gamma_{pe} = \gamma_r(2n_p + 1)$ and $\Gamma_{pp} = \gamma_c - \gamma_r(2n_e - n_0)$ are the small-signal coefficients, with n_e and n_p being the average number of carriers and photons, respectively. The damping rate, γ , and the square, ω_R^2 , of the relaxation resonance frequency read $\gamma = \Gamma_{ee} + \Gamma_{pp}$ and $\omega_R^2 = \Gamma_{ee}\Gamma_{pp} + \Gamma_{pe}\Gamma_{ep}$, respectively. We note that the small-signal coefficient γ_{ij} determines how fast carriers ($i=e$) and photons ($i=p$) respond to the variation in the number of carriers ($j=e$) and photons ($j=p$).

The Langevin noise force on the number of carriers, $F_e(t)$, and photons, $F_p(t)$, have auto-correlations given by $\langle F_e(t)F_e(t-\tau) \rangle = 2D_{ee}\delta(\tau)$ and $\langle F_p(t)F_p(t-\tau) \rangle = 2D_{pp}\delta(\tau)$, respectively, with $2D_{ee} = \gamma_p(n_0 - n_e) + \gamma_t n_e + \gamma_r n_0 n_p$ and $2D_{pp} = \gamma_c n_p + \gamma_r n_e + \gamma_r n_0 n_p$. The cross-correlation, instead, is $\langle F_p(t)F_e(t-\tau) \rangle = 2D_{pe}\delta(\tau)$, with $2D_{pe} = -\gamma_r n_0 n_p - \gamma_r n_e$.

ACKNOWLEDGEMENTS

Authors gratefully acknowledge funding by the European Research Council (ERC) under the European Union's Horizon 2020 Research and Innovation Programme (Grant No. 834410 FANO), and the Danish National Research Foundation (Grant No. DNRF147 NanoPhoton). Y.Y. acknowledges the support from Villum Fonden via the Young Investigator Programme (Grant No. 42026).

[1] J. Hecht, *Appl. Opt.* **49**, F99 (2010).
[2] M. T. Hill and M. C. Gather, *Nature Photonics* **8**, 908 (2014).
[3] C.-Z. Ning, *Advanced Photonics* **1**, 014002 (2019).
[4] R.-M. Ma and R. F. Oulton, *Nature Nanotechnology* **14**, 12 (2019).
[5] H. Deng, G. L. Lippi, J. Mørk, J. Wiersig, and S. Reitzenstein, *Advanced Optical Materials* **9**, 2100415 (2021).
[6] Z. Zhang, L. Nest, S. Wang, S.-Y. Wang, and R.-M. Ma, *Photon. Res.* **9**, 1699 (2021).
[7] S. Kreinberg, T. Grbešić, M. Straufš, A. Carmele, M. Emmerling, C. Schneider, S. Höfling, X. Porte, and S. Reitzenstein, *Light: Science & Applications* **7**, 41 (2018).
[8] Z. Zhang, H. Zhao, S. Wu, T. Wu, X. Qiao, Z. Gao, R. Agarwal, S. Longhi, N. M. Litchinitser, L. Ge, and L. Feng, *Nature* **612**, 246 (2022).
[9] B. J. Shastri, A. N. Tait, T. Ferreira de Lima, W. H. P. Pernice, H. Bhaskaran, C. D. Wright, and P. R. Prucnal, *Nature Photonics* **15**, 102 (2021).
[10] K. Nozaki, S. Matsuo, T. Fujii, K. Takeda, A. Shinya, E. Kuramochi, and M. Notomi, *Nature Photonics* **13**, 454 (2019).
[11] K. Takeda, T. Tsurugaya, T. Fujii, A. Shinya, Y. Maeda, T. Tsuchizawa, H. Nishi, M. Notomi, T. Kakitsuka, and S. Matsuo, *Opt. Express* **29**, 26082 (2021).
[12] D. A. B. Miller, *J. Lightwave Technol.* **35**, 346 (2017).
[13] S. Hu and S. M. Weiss, *ACS Photonics* **3**, 1647 (2016).
[14] H. Choi, M. Heuck, and D. Englund, *Phys. Rev. Lett.* **118**, 223605 (2017).
[15] F. Wang, R. E. Christiansen, Y. Yu, J. Mørk, and O. Sigmund, *Applied Physics Letters* **113**, 241101 (2018).
[16] M. Albrechtsen, B. Vosoughi Lahijani, R. E. Christiansen, V. T. H. Nguyen, L. N. Cassee, S. E. Hansen,

N. Stenger, O. Sigmund, H. Jansen, J. Mørk, and S. Stobbe, *Nature Communications* **13**, 6281 (2022).

[17] M. Albrechtsen, B. V. Lahijani, and S. Stobbe, *Opt. Express* **30**, 15458 (2022).

[18] G. Kountouris, J. Mørk, E. V. Denning, and P. T. Kristensen, *Opt. Express* **30**, 40367 (2022).

[19] P. T. Kristensen, C. V. Vlack, and S. Hughes, *Opt. Lett.* **37**, 1649 (2012).

[20] C. Sauvan, J. P. Hugonin, I. S. Maksymov, and P. Lalanne, *Phys. Rev. Lett.* **110**, 237401 (2013).

[21] R. Cocciali, M. Boroditsky, K. Kim, Y. Rahmat-Samii, and E. Yablonovitch, *IEE Proceedings - Optoelectronics* **145**, 391 (1998).

[22] J. B. Khurgin, *Nature Nanotechnology* **10**, 2 (2015).

[23] S. I. Bozhevolnyi and J. B. Khurgin, *Optica* **3**, 1418 (2016).

[24] A. Higuera-Rodriguez, B. Romeira, S. Birindelli, L. E. Black, E. Smalbrugge, P. J. van Veldhoven, W. M. M. Kessels, M. K. Smit, and A. Fiore, *Nano Letters* **17**, 2627 (2017).

[25] P. R. Rice and H. J. Carmichael, *Phys. Rev. A* **50**, 4318 (1994).

[26] L. A. Coldren, S. W. Corzine, and M. Mašanović, *Diode Lasers and Photonic Integrated Circuits*, 2nd ed. (John Wiley & Sons, Inc., 2012).

[27] C. Z. Ning, *IEEE Journal of Selected Topics in Quantum Electronics* **19**, 1503604 (2013).

[28] S. Strauf, K. Hennessy, M. T. Rakher, Y.-S. Choi, A. Badolato, L. C. Andreani, E. L. Hu, P. M. Petroff, and D. Bouwmeester, *Phys. Rev. Lett.* **96**, 127404 (2006).

[29] S. M. Ulrich, C. Gies, S. Ates, J. Wiersig, S. Reitzenstein, C. Hofmann, A. Löffler, A. Forchel, F. Jahnke, and P. Michler, *Phys. Rev. Lett.* **98**, 043906 (2007).

[30] S. H. Pan, Q. Gu, A. E. Amili, F. Vallini, and Y. Fainman, *Optica* **3**, 1260 (2016).

[31] S. Kreinberg, W. W. Chow, J. Wolters, C. Schneider, C. Gies, F. Jahnke, S. Höfling, M. Kamp, and S. Reitzenstein, *Light: Science & Applications* **6**, e17030 (2017).

[32] N. Takemura, M. Takiguchi, E. Kuramochi, A. Shinya, T. Sato, K. Takeda, S. Matsuo, and M. Notomi, *Phys. Rev. A* **99**, 053820 (2019).

[33] M. Fox, *Quantum Optics: An Introduction* (Oxford University Press, 2006).

[34] B. Korzh, Q.-Y. Zhao, J. P. Allmaras, S. Frasca, T. M. Autry, E. A. Bersin, A. D. Beyer, R. M. Briggs, B. Bumble, M. Colangelo, G. M. Crouch, A. E. Dane, T. Gerrits, A. E. Lita, F. Marsili, G. Moody, C. Peña, E. Ramirez, J. D. Rezac, N. Sinclair, M. J. Stevens, A. E. Velasco, V. B. Verma, E. E. Wollman, S. Xie, D. Zhu, P. D. Hale, M. Spiropulu, K. L. Silverman, R. P. Mirin, S. W. Nam, A. G. Kozorezov, M. D. Shaw, and K. K. Berggren, *Nature Photonics* **14**, 250 (2020).

[35] S. T. Jagsch, N. V. Triviño, F. Lohof, G. Callsen, S. Kalinowski, I. M. Rousseau, R. Barzel, J.-F. Carlin, F. Jahnke, R. Butté, C. Gies, A. Hoffmann, N. Grandjean, and S. Reitzenstein, *Nature Communications* **9**, 564 (2018).

[36] F. Lohof, R. Barzel, P. Gartner, and C. Gies, *Phys. Rev. Appl.* **10**, 054055 (2018).

[37] M. A. Carroll, G. D'Alessandro, G. L. Lippi, G.-L. Oppo, and F. Papoff, *Phys. Rev. Lett.* **126**, 063902 (2021).

[38] A. A. Vyshnevyy and D. Y. Fedyanin, *Phys. Rev. Lett.* **128**, 029401 (2022).

[39] G. Lippi, T. Wang, and G. Puccioni, *Chaos, Solitons & Fractals* **157**, 111850 (2022).

[40] M. A. Carroll, G. D'Alessandro, G. L. Lippi, G.-L. Oppo, and F. Papoff, *Phys. Rev. Lett.* **128**, 029402 (2022).

[41] A. M. Yacomotti, Z. Denis, A. Biella, and C. Ciuti, *Laser & Photonics Reviews* **17**, 2200377 (2022).

[42] Y. Yamamoto and G. Björk, *Japanese Journal of Applied Physics* **30**, L2039 (1991).

[43] G. Björk and Y. Yamamoto, *IEEE Journal of Quantum Electronics* **27**, 2386 (1991).

[44] J. Mørk and G. L. Lippi, *Applied Physics Letters* **112**, 141103 (2018).

[45] E. C. André, J. Mørk, and M. Wubs, *Opt. Express* **28**, 32632 (2020).

[46] M. Bündgaard-Nielsen, E. V. Denning, M. Saldutti, and J. Mørk, arXiv:2301.11815 (2023), 10.48550/ARXIV.2301.11815.

[47] G. Björk, A. Karlsson, and Y. Yamamoto, *Phys. Rev. A* **50**, 1675 (1994).

[48] R. Jin, D. Boggavarapu, M. Sargent, P. Meystre, H. M. Gibbs, and G. Khitrova, *Phys. Rev. A* **49**, 4038 (1994).

[49] R.-M. Ma, R. F. Oulton, V. J. Sorger, and X. Zhang, *Laser & Photonics Reviews* **7**, 1 (2013).

[50] M. Notomi, *Reports on Progress in Physics* **73**, 096501 (2010).

[51] S. A. Maier, *Plasmonics: Fundamentals and Applications* (Springer New York, NY, 2007).

[52] F. Wang and Y. R. Shen, *Phys. Rev. Lett.* **97**, 206806 (2006).

[53] M. Saldutti, M. Xiong, E. Dimopoulos, Y. Yu, M. Gioannini, and J. Mørk, *Nanomaterials* **11** (2021), 10.3390/nano11113030.

[54] T. Asano, Y. Ochi, Y. Takahashi, K. Kishimoto, and S. Noda, *Opt. Express* **25**, 1769 (2017).

[55] Z. Zhang and M. Qiu, *Opt. Express* **12**, 3988 (2004).

[56] M. Nomura, N. Kumagai, S. Iwamoto, Y. Ota, and Y. Arakawa, *Nature Physics* **6**, 279 (2010).

[57] P. Lodahl, S. Mahmoodian, and S. Stobbe, *Rev. Mod. Phys.* **87**, 347 (2015).

[58] M. Takiguchi, S. Sasaki, K. Tateno, E. Chen, K. Nozaki, S. Sergeant, E. Kuramochi, G. Zhang, A. Shinya, and M. Notomi, *ACS Photonics* **7**, 3467 (2020).

[59] M. Ono, M. Hata, M. Tsunekawa, K. Nozaki, H. Sumikura, H. Chiba, and M. Notomi, *Nature Photonics* **14**, 37 (2020).

[60] M. Saldutti, Y. Yu, P. T. Kristensen, G. Kountouris, and J. Mørk, in *2022 IEEE Photonics Conference (IPC)* (2022) pp. 1–2.

[61] J. Mørk and K. Yvind, *Optica* **7**, 1641 (2020).

[62] J. D. Jackson, *Classical electrodynamics*, 3rd ed. (John Wiley & Sons, Inc., 1999).

[63] B. Romeira and A. Fiore, *IEEE Journal of Quantum Electronics* **54**, 1 (2018).

[64] M. Nomura, N. Kumagai, S. Iwamoto, Y. Ota, and Y. Arakawa, *Opt. Express* **17**, 15975 (2009).

[65] J.-M. Gérard, “Solid-state cavity-quantum electrodynamics with self-assembled quantum dots,” in *Single Quantum Dots: Fundamentals, Applications, and New Concepts* (Springer Berlin Heidelberg, Berlin, Heidelberg, 2003) pp. 269–314.

[66] P. Lalanne, W. Yan, K. Vynck, C. Sauvan, and J.-P. Hugonin, *Laser & Photonics Reviews* **12**, 1700113 (2018).

[67] P. T. Kristensen, K. Herrmann, F. Intravaia, and K. Busch, *Adv. Opt. Photon.* **12**, 612 (2020).

[68] J. Jensen and O. Sigmund, *Laser & Photonics Reviews* **5**, 308 (2011).

[69] E. Kuramochi, H. Duprez, J. Kim, M. Takiguchi, K. Takeda, T. Fujii, K. Nozaki, A. Shinya, H. Sumikura, H. Taniyama, S. Matsuo, and M. Notomi, *Opt. Express* **26**, 26598 (2018).

[70] E. Dimopoulos, A. Sakanas, A. Marchevsky, M. Xiong, Y. Yu, E. Semenova, J. Mørk, and K. Yvind, *Laser & Photonics Reviews* **n/a**, 2200109.

[71] M. Lørke, T. Suhr, N. Gregersen, and J. Mørk, *Phys. Rev. B* **87**, 205310 (2013).

[72] J. B. Khurgin and M. A. Noginov, *Laser & Photonics Reviews* **15**, 2000250 (2021).

[73] C. Gies, J. Wiersig, M. Lørke, and F. Jahnke, *Phys. Rev. A* **75**, 013803 (2007).

[74] A. Auffèves, D. Gerace, J.-M. Gérard, M. F. Santos, L. C. Andreani, and J.-P. Poizat, *Phys. Rev. B* **81**, 245419 (2010).

[75] A. Moelbjerg, P. Kaer, M. Lørke, B. Tromborg, and J. Mørk, *IEEE Journal of Quantum Electronics* **49**, 945 (2013).

[76] C. Gies, F. Gericke, P. Gartner, S. Holzinger, C. Hopfmann, T. Heindel, J. Wolters, C. Schneider, M. Florian, F. Jahnke, S. Höfling, M. Kamp, and S. Reitzenstein, *Phys. Rev. A* **96**, 023806 (2017).

[77] F. Jahnke, C. Gies, M. Aßmann, M. Bayer, H. A. M. Leymann, A. Foerster, J. Wiersig, C. Schneider, M. Kamp, and S. Höfling, *Nature Communications* **7**, 11540 (2016).

[78] S. Matsuo, T. Sato, K. Takeda, A. Shinya, K. Nozaki, H. Taniyama, M. Notomi, K. Hasebe, and T. Kakitsuka, *IEEE Journal of Selected Topics in Quantum Electronics* **19**, 4900311 (2013).

[79] Y. Ota, M. Kakuda, K. Watanabe, S. Iwamoto, and Y. Arakawa, *Opt. Express* **25**, 19981 (2017).

[80] T. Zhou, M. Tang, H. Li, Z. Zhang, Y. Cui, J.-S. Park, M. Martin, T. Baron, S. Chen, H. Liu, and Z. Zhang, *IEEE Journal of Selected Topics in Quantum Electronics* **28**, 1 (2022).

[81] N. Gregersen, T. Suhr, M. Lørke, and J. Mørk, *Applied Physics Letters* **100**, 131107 (2012).

[82] J. Mark and J. Mørk, *Applied Physics Letters* **61**, 2281 (1992).

[83] Y. Yamamoto, S. Machida, and O. Nilsson, *Phys. Rev. A* **34**, 4025 (1986).

[84] K. Roy-Choudhury and A. F. J. Levi, *Phys. Rev. A* **81**, 013827 (2010).

[85] D. T. Gillespie, *Journal of Computational Physics* **22**, 403 (1976).

[86] G. P. Puccioni and G. L. Lippi, *Opt. Express* **23**, 2369 (2015).

[87] P. Gartner, *Phys. Rev. A* **84**, 053804 (2011).

[88] M. Yamada, *Theory of Semiconductor Lasers: From Basis of Quantum Electronics to Analyses of the Mode Competition Phenomena and Noise* (Springer Japan, Tokyo, 2014).

[89] P. Borri, W. Langbein, J. M. Hvam, F. Heinrichsdorff, M.-H. Mao, and D. Bimberg, *Applied Physics Letters* **76**, 1380 (2000).

[90] C. Henry, *Journal of Lightwave Technology* **4**, 298 (1986).

[91] A. L. Schawlow and C. H. Townes, *Phys. Rev.* **112**, 1940 (1958).

[92] C. Henry, *IEEE Journal of Quantum Electronics* **18**, 259 (1982).

[93] A. Pick, A. Cerjan, D. Liu, A. W. Rodriguez, A. D. Stone, Y. D. Chong, and S. G. Johnson, *Phys. Rev. A* **91**, 063806 (2015).

[94] A. Cerjan, A. Pick, Y. D. Chong, S. G. Johnson, and A. D. Stone, *Opt. Express* **23**, 28316 (2015).

[95] T. Wang, J. Zou, G. P. Puccioni, W. Zhao, X. Lin, H. Chen, G. Wang, and G. L. Lippi, *Opt. Express* **29**, 5081 (2021).

[96] S. Noda, *Science* **314**, 260 (2006).

[97] D. Kleppner, *Phys. Rev. Lett.* **47**, 233 (1981).

[98] E. Yablonovitch, *Phys. Rev. Lett.* **58**, 2059 (1987).

[99] Y. Yamamoto, S. Machida, and G. Björk, *Phys. Rev. A* **44**, 657 (1991).

[100] E. V. Denning, J. Iles-Smith, A. D. Osterkryger, N. Gregersen, and J. Mørk, *Phys. Rev. B* **98**, 121306 (2018).

[101] T. Baba, T. Hamano, F. Koyama, and K. Iga, *IEEE Journal of Quantum Electronics* **27**, 1347 (1991).

[102] S. Noda, M. Fujita, and T. Asano, *Nature Photonics* **1**, 449 (2007).

[103] M. Takiguchi, H. Taniyama, H. Sumikura, M. D. Birowosuto, E. Kuramochi, A. Shinya, T. Sato, K. Takeda, S. Matsuo, and M. Notomi, *Opt. Express* **24**, 3441 (2016).

[104] S. Gwo and C.-K. Shih, *Reports on Progress in Physics* **79**, 086501 (2016).

[105] N. Takemura, M. Takiguchi, and M. Notomi, *J. Opt. Soc. Am. B* **38**, 699 (2021).

[106] M. O. Scully and W. E. Lamb, *Phys. Rev.* **159**, 208 (1967).

[107] Y. Xu, R. K. Lee, and A. Yariv, *Phys. Rev. A* **61**, 033807 (2000).

[108] L. Novotny and B. Hecht, *Principles of Nano-Optics* (Cambridge University Press, 2006).

[109] R. K. Chang and A. J. Campillo, *Optical processes in microcavities* (London, 1996).

[110] A. W. Snyder and J. D. Love, *Optical Waveguide Theory* (Springer New York, NY, 1983).

[111] P. T. Kristensen, R.-C. Ge, and S. Hughes, *Phys. Rev. A* **92**, 053810 (2015).

[112] E. A. Muljarov and W. Langbein, *Phys. Rev. A* **96**, 017801 (2017).

[113] P. T. Kristensen, R.-C. Ge, and S. Hughes, *Phys. Rev. A* **96**, 017802 (2017).

- [114] J. D. Joannopoulos, S. G. Johnson, J. N. Winn, and R. D. Meade, *Photonic Crystals: Molding the Flow of Light - Second Edition*, rev - revised, 2 ed. (Princeton University Press, 2008).
- [115] R. El-Ganainy, K. G. Makris, M. Khajavikhan, Z. H. Musslimani, S. Rotter, and D. N. Christodoulides, Nature Physics **14**, 11 (2018).
- [116] E. Purcell, Phys. Rev. **69**, 674 (1946).
- [117] T. Suhara, *Semiconductor Laser Fundamentals*, 1st ed. (CRC Press, 2004).
- [118] A. Sobiesierski and P. Smowton (Elsevier, Amsterdam, 2011) pp. 353–384.